

Existence of the critical endpoint in the vector meson extended linear sigma model

P. Kovács,^{1,*} Zs. Szép,^{2,†} and Gy. Wolf^{3,‡}

¹*Institute for Particle and Nuclear Physics, Wigner Research Centre for Physics,
Hungarian Academy of Sciences, H-1525 Budapest, Hungary*

²*MTA-ELTE Statistical and Biological Physics Research Group, H-1117 Budapest, Hungary*

³*Institute for Particle and Nuclear Physics, Wigner Research Center for Physics,
Hungarian Academy of Sciences, H-1525 Budapest, Hungary*

The chiral phase transition of the strongly interacting matter is investigated at nonzero temperature and baryon chemical potential (μ_B) within an extended $(2+1)$ flavor Polyakov constituent quark-meson model that incorporates the effect of the vector and axial vector mesons. The effect of the fermionic vacuum and thermal fluctuations computed from the grand potential of the model is taken into account in the curvature masses of the scalar and pseudoscalar mesons. The parameters of the model are determined by comparing masses and tree-level decay widths with experimental values in a χ^2 -minimization procedure that selects between various possible assignments of scalar nonet states to physical particles. We examine the restoration of the chiral symmetry by monitoring the temperature evolution of condensates and the chiral partners' masses and of the mixing angles for the pseudoscalar $\eta-\eta'$ and the corresponding scalar complex. We calculate the pressure and various thermodynamical observables derived from it and compare them to the continuum extrapolated lattice results of the Wuppertal-Budapest collaboration. We study the $T-\mu_B$ phase diagram of the model and find that a critical endpoint exists for parameters of the model, which give acceptable values of χ^2 .

PACS numbers: 12.39.Fe, 11.30.Rd, 11.30.Qc, 14.40.Be

I. INTRODUCTION

We investigate properties of the strongly interacting matter at high temperature and/or density. Currently, the strong matter can be accessed experimentally at low density (RHIC/Brookhaven and LHC/CERN) and at normal nuclear density (ordinary nuclear physics). Its properties at high densities, where the critical endpoint (CEP) probably sits, are not known, neither experimentally nor theoretically. The theory of the strongly interacting matter (QCD) can be solved perturbatively only at very high energies, not relevant for the problems here. Lattice computations based on importance sampling face serious difficulties at finite, especially large density. Therefore, we are left with effective models, in which certain aspects of the strongly interacting matter can be studied. The underlying principle in the construction of such models is that they share the same global symmetries as the QCD. There are different ways in which the chiral symmetry can be realized. At large temperatures and densities, one expects the chiral symmetry of QCD to be restored. Then, chiral partners have to become degenerate in mass, e.g., the sigma meson and the pions. To investigate the mechanism of chiral symmetry restoration, effective theories with linearly realized chiral symmetry are most appropriate.

In [1] an extended linear sigma model (EL σ M) with $U(3)_L \times U(3)_R$ global symmetry was developed, which

incorporates the vector and axial vector mesons. The parametrization of the EL σ M performed at vanishing temperature shows that the scalar states are preferred as $\bar{q}q$ states only if their masses are above 1 GeV with an opposite ordering $m_{a_0} < m_{K_0^*}$ compared to the corresponding experimental values. QCD sum rule analyses based on Borel transformed two-point correlation functions of $\bar{q}q$ currents also predict the masses of $\sigma \equiv f_0^{L(ow)}$ (the scalar particle with nonstrange quark content)¹ and a_0 to be around 1.2 GeV and larger masses for K_0^* and the other f_0 —the $f_0^{H(igh)}$ — of the nonet, due to the strange quark content of the latter (for details see [3] and references therein). Only when the above QCD sum rule analysis is done with tetraquark currents are the masses of scalar mesons obtained in the region 0.6 – 1.0 GeV with the ordering $m_{f_0^L} < m_{K_0^*} < m_{f_0^H, a_0}$ [3–5].

Since the mass of the f_0^L , the excitation of the vacuum with quantum numbers $J^{PC} = 0^{++}$, is intimately related to the nonstrange condensate, one could expect in the context of the EL σ M that a parametrization leading to a large f_0^L mass will result in a high pseudocritical temperature. This is because in the case of a smooth crossover phase transition the larger the f_0^L mass compared to the mass of its chiral partner, that is the pion, the larger is the temperature at which $m_{f_0^L}$ approaches m_π in the process of the chiral symmetry restoration during which the value of the nonstrange condensate diminishes. Another problem with a large f_0^L mass when the thermodynamics

* kovacs.peter@wigner.mta.hu

† szepzs@achilles.elte.hu

‡ wolf.gyorgy@wigner.mta.hu

¹ From now on we always use f_0^L instead of σ , as in the Particle Data Group (PDG) [2].

of the $\text{EL}\sigma\text{M}$ is studied comes from the fact that usually the first order phase transition, which occurs at $T = 0$ as the baryon chemical potential is increased, weakens with increasing values of the f_0^L mass and eventually becomes a crossover at a high enough value of $m_{f_0^L}$ [6, 7]. All this suggests that even if a zero temperature analysis, which excludes the f_0^L and f_0^H scalar mesons from the parametrization process favors the heavy scalars as $\bar{q}q$ states, the combined zero and finite temperature analysis can give a different result in a given approximate solution of the model. To completely clarify this issue, it seems necessary to include in the model all the physical scalar states below 2 GeV, which is a task we plan to do in a later work along the line of [8].

Beside the restoration of the chiral symmetry, the liberation of quarks also occurs in QCD at high temperature and/or density. The order parameter of this deconfinement phase transition in the pure gauge theory is the Polyakov loop. It is therefore reasonable to include it in our model in the hope (supported by existing results in the literature) that in this way a better phenomenological description of the strongly interacting matter can be achieved.

We shall study the thermodynamics of the (2+1) flavor Polyakov quark meson model in which, beyond the vector and axial vector mesons included alongside the scalar and pseudoscalar ones, we take into account, as fermionic degrees of freedom, the constituent quarks propagating on a constant gluon background in the temporal direction, which naturally leads in a mean-field treatment to the appearance of the Polyakov loop. The influence of the fermionic vacuum fluctuations on the thermodynamics of the Polyakov loop extended quark meson (PQM) model proved to be very important. In the case of two flavors ($N_f = 2$) it was shown in [9] that their inclusion can change the order of the phase transition at vanishing baryon chemical potential μ_B and that renormalization is required to guarantee the second order nature of the temperature driven phase transition in the chiral limit. In the PQM model the effect of the fermionic vacuum fluctuations on the $T - \mu_B$ phase diagram was investigated, e.g., in [10] for $N_f = 2$ and in [7, 11] for $N_f = 2 + 1$. We shall incorporate the vacuum fluctuations of the fermions in the grand potential and study the effect of the inclusion of the (axial) vector mesons by comparing thermodynamic quantities and the $T - \mu_B$ phase diagram with those determined in the literature in the context of the PQM model.

For $N_f = 2$ and without the inclusion of fermions, the restoration of chiral symmetry at high temperature was studied within the $\text{EL}\sigma\text{M}$ in Ref. [12], using the functional renormalization group approach, and in the gauged version of the model in [13], using the Cornwall-Jackiw-Tomboulis formalism [14]. An application of the (2+1)-flavor $\text{EL}\sigma\text{M}$ to an in-medium study was reported in [15]. In contrast to this latter reference, in which it is

also rather obscure how thermal corrections are included in the mass of the (axial-)vectors, in the present work we properly take into account the wave function renormalization factors (neglected in [15]), which are related to the redefinition of the (axial-)vector fields and use a complete set of parameters obtained from a consistent parametrization of the model.

The paper is organized as follows. In Sec. II we introduce the model, giving the Lagrangian and the Polyakov loop potentials considered in this study. In Sec. III we introduce the grand potential, the approximation used for its computation, summarize the determination of the curvature masses and of the renormalization of the fermion vacuum fluctuations and present the field equations to be solved numerically. The determination of the model parameters, which is based on a χ^2 -minimization procedure, is described in detail in Sec. IV. In Sec. V we present our results concerning the medium mass variation of the model constituents, the thermodynamics quantities derived from the pressure, and the $T - \mu_B$ phase diagram. We conclude in Sec. VI.

II. FORMULATION OF THE MODEL

In this section we give the Lagrangian of the model, introduce the Polyakov loop, and present the different forms of the Polyakov loop potential we shall use later. We work with a modified version of the chiral Lagrangian rather than the one employed in [1] at zero temperature (more details on the construction of chiral Lagrangians can be found in [16–18]). We consider now a different $U_A(1)$ anomaly term (term with c_1), because this term contains the fields with lower powers than the one used in [1], while it does not affect the zero temperature properties much (see [19]). Moreover, we introduce additional kinetic and Yukawa coupling terms for the constituent fermions $\Psi = (q_u, q_d, q_s)^T$. Another important modification is the presence of the gluon field in the covariant derivative of the quark field. In the mean-field approximation, this will give rise in the grand potential of Sec. III to the appearance of the Polyakov loop, which mimics some properties of the quark confinement. Moreover, since $2 \rightarrow 2$ (axial) vector scattering processes will not be considered here, the purely four field (axial) vector self-interaction terms are left out (see [1] for the complete Lagrangian).

A. Lagrangian of the PQM with (axial) vector mesons

According to the considerations above, the Lagrangian we shall use has the following form:

$$\begin{aligned} \mathcal{L} = & \text{Tr}[(D_\mu M)^\dagger (D_\mu M)] - m_0^2 \text{Tr}(M^\dagger M) - \lambda_1 [\text{Tr}(M^\dagger M)]^2 - \lambda_2 \text{Tr}(M^\dagger M)^2 + c_1 (\det M + \det M^\dagger) + \text{Tr}[H(M + M^\dagger)] \\ & - \frac{1}{4} \text{Tr}(L_{\mu\nu}^2 + R_{\mu\nu}^2) + \text{Tr} \left[\left(\frac{m_1^2}{2} + \Delta \right) (L_\mu^2 + R_\mu^2) \right] + i \frac{g_2^2}{2} (\text{Tr}\{L_{\mu\nu}[L^\mu, L^\nu]\} + \text{Tr}\{R_{\mu\nu}[R^\mu, R^\nu]\}) \\ & + \frac{h_1}{2} \text{Tr}(M^\dagger M) \text{Tr}(L_\mu^2 + R_\mu^2) + h_2 \text{Tr}(|L_\mu M|^2 + |MR_\mu|^2) + 2h_3 \text{Tr}(L_\mu M R^\mu M^\dagger) + \bar{\Psi} [i\gamma_\mu D^\mu - \mathcal{M}] \Psi. \end{aligned} \quad (1)$$

The covariant derivatives appearing in (1) are written in terms of the electromagnetic field A_e^μ , the left- and right-handed vector fields L^μ, R^μ and the gluon fields G_i^μ as

$$D^\mu M = \partial^\mu M - ig_1(L^\mu M - MR^\mu) - ieA_e^\mu[T_3, M], \quad D^\mu \Psi = \partial^\mu \Psi - iG^\mu \Psi, \quad (2)$$

where $G^\mu = g_s G_i^\mu T_i$, with $T_i = \lambda_i/2$ ($i = 1, \dots, 8$) denoting the $SU(3)$ group generators given in terms of the Gell-Mann matrices λ_i . The field strength tensors

$$L^{\mu\nu} = \partial^\mu L^\nu - ieA_e^\mu[T_3, L^\nu] - \{\partial^\nu L^\mu - ieA_e^\nu[T_3, L^\mu]\}, \quad R^{\mu\nu} = \partial^\mu R^\nu - ieA_e^\mu[T_3, R^\nu] - \{\partial^\nu R^\mu - ieA_e^\nu[T_3, R^\mu]\}, \quad (3)$$

are constructed from the left- and right-handed vector fields L^μ and R^μ which contain the nonets of vector (V_a^μ) and axial vector (A_a^μ) meson fields as follows:

$$L^\mu \equiv V^\mu + A^\mu \equiv \sum_{a=0}^8 (V_a^\mu + A_a^\mu) T_a = \frac{1}{\sqrt{2}} \begin{pmatrix} \frac{\omega_N + \rho^0}{\sqrt{2}} + \frac{f_{1N} + a_1^0}{\sqrt{2}} & \rho^+ + a_1^+ & K^{*+} + K_1^+ \\ \rho^- + a_1^- & \frac{\omega_N - \rho^0}{\sqrt{2}} + \frac{f_{1N} - a_1^0}{\sqrt{2}} & K^{*0} + K_1^0 \\ K^{*-} + K_1^- & \bar{K}^{*0} + \bar{K}_1^0 & \omega_S + f_{1S} \end{pmatrix}^\mu, \quad (4)$$

$$R^\mu \equiv V^\mu - A^\mu \equiv \sum_{a=0}^8 (V_a^\mu - A_a^\mu) T_a = \frac{1}{\sqrt{2}} \begin{pmatrix} \frac{\omega_N + \rho^0}{\sqrt{2}} - \frac{f_{1N} + a_1^0}{\sqrt{2}} & \rho^+ - a_1^+ & K^{*+} - K_1^+ \\ \rho^- - a_1^- & \frac{\omega_N - \rho^0}{\sqrt{2}} - \frac{f_{1N} - a_1^0}{\sqrt{2}} & K^{*0} - K_1^0 \\ K^{*-} - K_1^- & \bar{K}^{*0} - \bar{K}_1^0 & \omega_S - f_{1S} \end{pmatrix}^\mu, \quad (5)$$

where the assignment to physical fields is made explicit with the exception of the mixing sector. The index $a = 0, \dots, 8$ runs over the generators of the $U(3)$ group which includes also $T_0 = \lambda_0/2$ with $\lambda_0 = \sqrt{\frac{2}{3}} \mathbf{1}_{3 \times 3}$. The matrix M in the Lagrangian collects the nonets of scalar (S_a) and pseudoscalar (P_a) meson fields,

$$M \equiv M_S + M_{PS} \equiv \sum_{a=0}^8 (S_a + iP_a) T_a = \frac{1}{\sqrt{2}} \begin{pmatrix} \frac{(\sigma_N + a_0^0) + i(\eta_N + \pi^0)}{\sqrt{2}} & a_0^+ + i\pi^+ & K_0^{*+} + iK^+ \\ a_0^- + i\pi^- & \frac{(\sigma_N - a_0^0) + i(\eta_N - \pi^0)}{\sqrt{2}} & K_0^{*0} + iK^0 \\ K_0^{*-} + iK^- & \bar{K}_0^{*0} + i\bar{K}^0 & \sigma_S + i\eta_S \end{pmatrix}, \quad (6)$$

while the external fields related to the scalar and vector fields are introduced with the following parametrization:

$$H = H_0 T_0 + H_8 T_8 = \frac{1}{2} \text{diag}(h_{0N}, h_{0N}, \sqrt{2} h_{0S}), \quad (7)$$

$$\Delta = \Delta_0 T_0 + \Delta_8 T_8 = \text{diag}(\delta_N, \delta_N, \delta_S). \quad (8)$$

The first line in the Lagrangian (1) contains the kinetic and self-interaction terms of the (pseudo)scalars together with a $U_A(1)$ anomaly term and an explicit symmetry breaking term. The second line consists of the kinetic terms for the (axial)vectors, altogether with explicit symmetry breaking terms for the (axial)vectors and the (axial)vector–electromagnetic interaction terms. In the third line one finds the (pseudo)scalar–(axial)vector interaction terms, the kinetic terms of the constituent quarks and their Yukawa-type interaction with the (pseudo)scalar mesons. The quark mass matrix

appearing there is defined as

$$\mathcal{M} = g_F (\mathbf{1}_{4 \times 4} M_S + i\gamma_5 M_{PS}), \quad (9)$$

and has the structure of a block matrix in flavor, Dirac, and color space.

For convenience, in the matrices above and throughout the article, we use the $N-S$ (nonstrange–strange) basis instead of the $0-8$ basis, which for a generic field $\xi_a \in (S_a, P_a, V_a^\mu, A_a^\mu, H_a, \Delta_a)$ is defined as

$$\xi_N = \frac{1}{\sqrt{3}} (\sqrt{2} \xi_0 + \xi_8), \quad \xi_S = \frac{1}{\sqrt{3}} (\xi_0 - \sqrt{2} \xi_8). \quad (10)$$

Since in the present work we neglect the isospin breaking, we have to deal with only two nonzero condensates (field expectation values), the $\phi_N \equiv \langle \sigma_N \rangle$ nonstrange and the $\phi_S \equiv \langle \sigma_S \rangle$ strange scalar condensates. In the broken symmetry phase, the model Lagrangian is obtained

with the usual procedure in which the nonstrange and strange scalar fields are shifted by their expectation values, $\sigma_{N/S} \rightarrow \sigma_{N/S} + \phi_{N/S}$, which will generate the tree-level masses and decay widths.

B. The Polyakov loop potential

The introduction of the Polyakov loop operator and its application in the present context can be found, for instance, in [20–22]. For the sake of completeness, however, let the key steps be presented here as well.

To go to finite temperature, analytic continuation to imaginary time should be performed, $t \rightarrow -i\tau$. The temporal component of the gluon gauge field, which is entering in the definition of the Polyakov loop operator, is transformed accordingly as $G_0(t, \mathbf{x}) \rightarrow -iG_4(\tau, \mathbf{x})$, while we assume that the spatial components of G^μ are vanishing. The Polyakov loop operator itself—which is nothing other than a path ordered Wilson loop of the gauge field in the temporal direction—is defined as [7, 23]

$$L = \mathcal{P} \exp \left(i \int_0^\beta d\tau G_4(\tau, \mathbf{x}) \right). \quad (11)$$

L and L^\dagger are matrices in the fundamental representation of the color gauge group $SU(N_c)$ with $N_c = 3$. Introducing the color traced Polyakov loops as

$$\Phi(\mathbf{x}) = \frac{1}{N_c} \text{Tr}_c L(\mathbf{x}), \quad \bar{\Phi}(\mathbf{x}) = \frac{1}{N_c} \text{Tr}_c L^\dagger(\mathbf{x}), \quad (12)$$

the Polyakov loop variables are defined as the thermal expectation values $\langle \Phi \rangle$ and $\langle \bar{\Phi} \rangle$. In the pure gauge case they are related to the free energy of infinitely heavy static quark and antiquarks.

As a next step, the so-called Polyakov gauge is chosen, in which $G_4(\tau, \mathbf{x}) = G_4(\mathbf{x})$ is time independent and diagonal in color space; that is, it belongs to the Cartan subalgebra. Furthermore, we approximate $G_4(\mathbf{x})$ to be homogeneous, thus it can be written as

$$G_4 = \phi_3 \lambda_3 + \phi_8 \lambda_8, \quad (13)$$

with ϕ_3 and ϕ_8 being real. Consequently, with these simplifications the Polyakov loop operator can be cast into the following form:

$$L = \text{diag}(z_1, z_2, z_1^{-1} z_2^{-1}), \quad (14)$$

with $z_1 = e^{i\beta(\phi_3 + \phi_8/\sqrt{3})}$, $z_2 = e^{i\beta(-\phi_3 + \phi_8/\sqrt{3})}$. When the constant diagonal G_4 , given in (13), is substituted into the kinetic term of the constituent quarks (2), the second term of the covariant derivative can be considered as a color dependent imaginary chemical potential. This observation is used for the calculation of the grand canonical potential in Sec. III.

The Polyakov loop potential describes the temperature driven deconfinement phase transition occurring in

the pure gauge theory; therefore, the potential is constructed using terms which are invariant under the $Z(3)$ symmetry, and some coefficient of these terms depend on the temperature in order to assure a nonzero expectation value of Φ at large temperature [24, 25]. The potential is constructed in such a way as to reproduce some thermodynamical quantities of the pure gauge theory computed on the lattice. For the functional form there are still various possibilities. The simplest polynomial potential introduced in [24] leads in Polyakov Nambu-Jona-Lasinio (PNJL) or PQM models to some unwanted properties, such as negative susceptibilities [26]. Therefore, we shall use a potential with a logarithmic form which is coming from the $SU(3)$ Haar measure of the group integration [27] and is free from the negative susceptibility problem. Moreover, as observed in [28], the trace anomaly calculated with the logarithmic parametrization of the Polyakov loop potential shows a better agreement with the corresponding quantity in the pure $SU(3)$ gauge theory computed recently on the lattice in [29], compared to the case when a polynomial Polyakov loop potential is used.

Although in thermodynamical applications the potential is a function of the expectation values $\langle \Phi \rangle$ and $\langle \bar{\Phi} \rangle$, we use for simplicity Φ and $\bar{\Phi}$ for its arguments. Then the logarithmic Polyakov loop potential can be written as

$$\beta^4 U_{\log}(\Phi, \bar{\Phi}) = -\frac{1}{2} a(T) \Phi \bar{\Phi} + b(T) \ln \left(1 - 6\Phi \bar{\Phi} + 4(\Phi^3 + \bar{\Phi}^3) - 3(\Phi \bar{\Phi})^2 \right), \quad (15)$$

with coefficients

$$a(T) = a_0 + a_1 \left(\frac{T_0}{T} \right) + a_2 \left(\frac{T_0}{T} \right)^2, \quad b(T) = b_3 \left(\frac{T_0}{T} \right)^3, \quad (16)$$

where the values of the constants are $a_0 = 3.51$, $a_1 = -2.47$, $a_2 = 15.22$, and $b_3 = -1.75$.

The above parametrization of the Polyakov loop potential does not include the backreaction of the dynamical quarks on the gauge sector and therefore the influence of the quarks on the deconfinement phase transition. This effect was discussed in [30] and in [28], where the dependence of T_0 on the number of quark flavors and the baryon chemical potential was estimated. This led to $T_0 = 187$ MeV for $m_s = 150$ MeV and $T_0 = 182$ MeV for $m_s = 95$ MeV. In the present study we shall use this latter value of T_0 . A refinement of this estimation was achieved in [28], where a quark-improved Polyakov loop potential was constructed by comparing the $SU(3)$ Yang-Mills (YM) effective potential with the gluonic effective potential computed with the functional renormalization group method by including the quark polarization in the gluon propagator. It was observed that the two potentials have the same shape and that they can be mapped into each other by relating the temperatures of the two systems, T_{YM} and T_{glue} , respectively. The use of the improved Polyakov loop potential U_{glue} was proposed in

[28], which, denoting by U_{YM} the potentials in (15), was constructed based on the relation

$$\frac{1}{T_{\text{glue}}^4} [U_{\text{glue}}(\Phi, \bar{\Phi})] \Big|_{t_{\text{glue}}} = \frac{1}{T_{\text{YM}}^4} [U_{\text{YM}}(\Phi, \bar{\Phi})] \Big|_{t_{\text{YM}}(t_{\text{glue}})}, \quad (17)$$

where the mapping between the reduced temperatures $t_{\text{YM}} = T_{\text{YM}}/T_c^{\text{YM}} - 1$ and $t_{\text{glue}} = T_{\text{glue}}/T_c^{\text{glue}} - 1$ was determined to be $t_{\text{YM}}(t_{\text{glue}}) \approx 0.57 t_{\text{glue}}$, with the critical temperatures $T_c^{\text{YM}} = 270$ MeV and $T_c^{\text{glue}} \in [180, 270]$ MeV. In practice this amounts to using in the right-hand side of (15), where T_0 means T_c^{YM} , the replacement $T \rightarrow T_c^{\text{YM}}(1 + 0.57(T/T_c^{\text{glue}} - 1))$ (on the left side of the arrow $T \equiv T_{\text{YM}}$, while on the right side $T \equiv T_{\text{glue}}$). In Sec. V we shall choose several values of T_c^{glue} in the range given above and study the sensitivity of the results to this parameter.

Before closing this section we mention that a gluonic potential with possible phenomenological applicability is also calculated in [31] in terms of the Polyakov loop variables $\langle \Phi \rangle$ and $\langle \bar{\Phi} \rangle$, using background field methods in the massive extension of the Landau-deWitt gauge.

III. THE GRAND POTENTIAL

To study the thermodynamics of a symmetric quark matter ($\mu_u = \mu_d = \mu_s \equiv \mu_q = \mu_B/3$), we shall use the grand potential $\Omega(T, \mu_q)$ obtained from the partition function of a three-dimensional spatially uniform system of volume V in thermal equilibrium at temperature $T = 1/\beta$. Following Ref. [32] the partition function can be given the following representation in terms of path integrals:

$$\begin{aligned} \mathcal{Z} &= e^{-\beta V \Omega(T, \mu_q)} = \text{Tr} \exp \left[-\beta \left(\hat{\mathcal{H}} - \sum_{f=u,d,s} \mu_f \hat{\mathcal{Q}}_f \right) \right] \\ &= \int \prod_{\text{PBC}} \mathcal{D}\xi_a \int \prod_{\text{APBC}} \mathcal{D}q_f \mathcal{D}q_f^\dagger \\ &\quad \times \exp \left[-\int_0^\beta d\tau \int_V d^3x \left(\mathcal{L} + \mu_q \sum_f q_f^\dagger q_f \right) \right], \quad (18) \end{aligned}$$

where (A)PBC stands for (anti)periodic boundary condition, $\hat{\mathcal{Q}}_f$ is the conserved charge operator, and ξ denotes here all the mesonic fields. Since the Polyakov loop is treated at mean-field level, there is no integration over the gluons [G_4 in (13) is a background field] and in this case the Polyakov loop potential (15) is simply added to the grand potential.

The simplest approximation for the evaluation of the grand potential frequently used in the literature takes into account the (pseudo)scalar mesons at mean-field level only. In the present case the vacuum and thermal fluctuations for the fermions are taken into account, while the mesonic vacuum fluctuations are neglected and the effects of the lightest mesonic thermal fluctuations (π , K ,

f_0^L) are included only in the pressure and the thermodynamical quantities derived from it. Therefore, the meson potential is classical (tree-level) and the fermion determinant obtained after performing the functional integration over the quark fields is evaluated for vanishing mesonic fluctuating fields. Since we would like to assess how the parametrization using vector and axial vector mesons influences the thermodynamics in this approximation, we shall also neglect the fluctuations of the vector and axial vector mesons. In this approximation, which we shall call *hybrid* (H) approximation, the grand potential reads

$$\Omega_{\text{H}}(T, \mu_q) = U(\langle M \rangle) + U(\langle \Phi \rangle, \langle \bar{\Phi} \rangle) + \Omega_{\bar{q}q}^{(0)}(T, \mu_q), \quad (19)$$

where $U(\langle M \rangle)$ is the tree-level meson potential, $U(\langle \Phi \rangle, \langle \bar{\Phi} \rangle)$ is the Polyakov loop potential and $\Omega_{\bar{q}q}^{(0)}$ is the contribution of the fermions for nonvanishing scalar backgrounds ϕ_N and ϕ_S and vanishing mesonic fluctuating fields, the case in which the quark mass matrix \mathcal{M} given in (9) is diagonal in flavor space. Note that \mathcal{M} has a nontrivial dependence on the scalar and pseudoscalar fluctuating fields, when they are nonvanishing.

The tree-level mesonic potential

$$\begin{aligned} U(\langle M \rangle) &= \frac{m_0^2}{2} (\phi_N^2 + \phi_S^2) - \frac{c_1}{2\sqrt{2}} \phi_N^2 \phi_S - h_S \phi_S - h_N \phi_N \\ &\quad + \frac{\lambda_1}{4} (\phi_N^2 + \phi_S^2)^2 + \frac{\lambda_2}{8} (\phi_N^4 + 2\phi_S^4) \\ &\quad + \frac{\delta m_0^2}{2} (\phi_N^2 + \phi_S^2) + \frac{\delta \lambda_2}{8} (\phi_N^4 + 2\phi_S^4), \quad (20) \end{aligned}$$

is obtained from the first line of (1) with the replacement $M, M^\dagger \rightarrow \langle M \rangle \equiv T_N \phi_N + T_S \phi_S$, where $T_{N/S} = \lambda_{N/S}/2$ with $\lambda_N = \text{diag}(1, 1, 0)$ and $\lambda_S = \text{diag}(0, 0, \sqrt{2})$. In the last line of (20) we explicitly added the counterterms which are needed to renormalize the fermionic vacuum fluctuations (see Sec. III A).

The contribution of the fermions to the grand potential in the approximation described above is obtained as

$$\begin{aligned} \mathcal{Z}_{\bar{q}q}^{(0)} &= e^{-\beta V \Omega_{\bar{q}q}^{(0)}} = \int \prod_{\text{APBC}} \mathcal{D}q_f \mathcal{D}q_f^\dagger \exp \left\{ \int_0^\beta d\tau \int_V d^3x \right. \\ &\quad \times q_f^\dagger \left[\left(i\gamma_0 \vec{\gamma} \cdot \vec{\nabla} - \frac{\partial}{\partial \tau} + \tilde{\mu}_q \right) \delta_{fg} - \gamma_0 \mathcal{M}_{fg} \Big|_{\xi_a=0} \right] q_g \Big\}, \quad (21) \end{aligned}$$

where summation over repeated indices $f, g \in \{u, d, s\}$ is understood, the superscript (0) reminds one that the mesonic fluctuating fields ξ_a are set to zero in the quark mass matrix \mathcal{M} defined in (9) and we introduced the color-dependent chemical potential $\tilde{\mu}_q = \mu_q - iG_4$, different for each color.

Evaluating the path integral in (21) as in [32] one obtains

$$\Omega_{\bar{q}q}^{(0)}(T, \mu_q) = \Omega_{\bar{q}q}^{(0)\text{v}} + \Omega_{\bar{q}q}^{(0)\text{T}}(T, \mu_q), \quad (22)$$

where the vacuum and thermal parts are, respectively,

$$\Omega_{\bar{q}q}^{(0)\text{v}} = -2N_c \sum_{f=u,d,s} \int \frac{d^3p}{(2\pi)^3} E_f(p), \quad (23)$$

$$\begin{aligned} \Omega_{\bar{q}q}^{(0)\text{T}}(T, \mu_q) = & -2T \sum_{j=1}^{N_c} \sum_{f=u,d,s} \int \frac{d^3p}{(2\pi)^3} \\ & \times [\ln(1 + e^{-\beta(E_f(p) - \tilde{\mu}_q^j)}) + \ln(1 + e^{-\beta(E_f(p) + \tilde{\mu}_q^j)})]. \end{aligned} \quad (24)$$

Here $\tilde{\mu}_q^j = \mu_q - i(G_4)_{jj}$, $E_f(p) = \sqrt{p^2 + m_f^2}$ with $p = |\mathbf{p}|$ and, in the nonstrange-strange basis, the constituent quark masses are given by

$$m_{u,d} = \frac{g_F}{2} \phi_N \quad \text{and} \quad m_s = \frac{g_F}{\sqrt{2}} \phi_S. \quad (25)$$

Writing

$$\sum_{j=1}^{N_c} \ln(1 + e^{-\beta(E_f(p) \mp \tilde{\mu}_q^j)}) = \text{Tr}_c \ln(1 + e^{\mp i\beta G_4} e^{-\beta E_f^\pm(p)}), \quad (26)$$

one recognizes the appearance of $L = e^{i\beta G_4}$ and $L^\dagger = e^{-i\beta G_4}$, given explicitly in (14). Using the properties $\det L = \det L^\dagger = 1$ and $L^\dagger L = 1$ one expresses (26) in terms of $\Phi = \text{Tr}_c L/3$ and $\bar{\Phi} = \text{Tr}_c L^\dagger/3$. We obtain

$$\Omega_{\bar{q}q}^{(0)\text{T}}(T, \mu_q) = -2T \sum_f \int \frac{d^3p}{(2\pi)^3} [\ln g_f^+(p) + \ln g_f^-(p)], \quad (27)$$

where $\Phi^+ = \bar{\Phi}$ and $\Phi^- = \Phi$ were introduced for convenience in order to write in a compact form

$$g_f^\pm(p) = 1 + 3 \left(\Phi^\pm + \Phi^\mp e^{-\beta E_f^\pm(p)} \right) e^{-\beta E_f^\pm(p)} + e^{-3\beta E_f^\pm(p)}, \quad (28)$$

with $E_f^\pm(p) = E_f(p) \mp \mu_f$.

A. Renormalization of the fermionic vacuum contribution

Using a three-dimensional cutoff Λ in the fermionic vacuum term (23), one obtains with the help of the mass formulas in (25)

$$\begin{aligned} -6 \sum_{f=u,d,s} \int \frac{d^3p}{(2\pi)^3} E_f(p) \theta(\Lambda - p) = & -\frac{9\Lambda^4}{4\pi^2} - \frac{3g_F^2}{8\pi^2} \Lambda^2 \\ & \times (\phi_N^2 + \phi_S^2) + \frac{3g_F^4}{64\pi^2} \ln\left(\frac{2\Lambda}{M_0 e^{\frac{1}{4}}}\right) (\phi_N^4 + 2\phi_S^4) \\ & - \frac{3}{8\pi^2} \sum_{f=u,d,s} m_f^4 \ln \frac{m_f}{M_0} + \mathcal{O}\left(\frac{m_f^6}{\Lambda^2}\right). \end{aligned} \quad (29)$$

The first term on the right-hand side, quartic in Λ , is uninteresting and can be removed from the potential by considering a subtracted potential such that the value of the

potential at $\phi_N = \phi_S = 0$ is subtracted. The quadratic and logarithmic divergences can be removed with the help of the counterterms in the tree-level mesonic potential (20) by choosing

$$\delta m_0^2 = \frac{3g_F^2}{4\pi^2} \Lambda^2 \quad \text{and} \quad \delta \lambda_2 = -\frac{3g_F^4}{8\pi^2} \ln \frac{2\Lambda}{M_0 e^{\frac{1}{4}}}. \quad (30)$$

Therefore, the renormalized fermionic vacuum contribution reads

$$\Omega_{\bar{q}q;R}^{(0)\text{v}} = -\frac{3}{8\pi^2} \sum_{f=u,d,s} m_f^4 \ln \frac{m_f}{M_0}. \quad (31)$$

It was shown in Refs. [7, 33] that the grand potential is independent of the renormalization scale, which means that $d\Omega_H/dM_0 \equiv 0$. The reason behind this is that after renormalization λ_2 becomes a quantity that depends on the renormalization scale M_0 and its β function is $\beta_{\lambda_2} = \frac{d\lambda_2}{d \ln M_0} = -\frac{3g_F^4}{8\pi^2}$, so that the M_0 dependence of λ_2 compensates the explicit dependence on M_0 of the renormalized vacuum term (31). As a consequence, we could freely choose the renormalization scale M_0 and maintain M_0 independency as long as we take into account the M_0 dependence of λ_2 (which means we cannot change M_0 and λ_2 independently). However, during the parametrization we scan through the parameter space uniformly treating all parameters independently; thus we do not use the M_0 dependence of λ_2 , but instead, we consider M_0 as one of the parameters (see Sec. IV for additional details).

B. The curvature meson masses

The squared masses of the scalar and pseudoscalar mesons, used later to determine the parameters of the model, are calculated from the elements of the corresponding curvature matrix, that is, the second derivative of the grand potential with respect to the mesonic fields, generally denoted by $\varphi_{i,a}$ in some appropriate basis indexed by a , with $i = S$ for scalar and $i = P$ for pseudoscalar mesons. These curvature matrices are symmetric and nondiagonal in the 0–8 or nonstrange–strange basis and can be decomposed as

$$m_{i,ab}^2 = \left. \frac{\partial^2 \Omega(T, \mu_q)}{\partial \varphi_{i,a} \partial \varphi_{i,b}} \right|_{\text{min}} = \mathbf{m}_{i,ab}^2 + \Delta m_{i,ab}^2 + \delta m_{i,ab}^2, \quad (32)$$

where the three terms on the right-hand side are as follows: $\mathbf{m}_{i,ab}^2$ is the tree-level mass matrix,² and $\Delta m_{i,ab}^2$ and $\delta m_{i,ab}^2$ are the contributions of the fermionic vacuum

² Compared to the case of the conventional $L\sigma M$, some elements of this matrix contain the wave-function renormalization constants $Z_\pi = Z_{\eta_N}, Z_K, Z_{\eta_S}, Z_{K_0^*}$, which are needed in order to maintain the canonical normalization of the fields in the presence of axial and vector mesons (see [1] for details).

TABLE I. The components of the pseudoscalar and scalar tree-level mass squared matrices and the corresponding contribution of the fermionic vacuum and thermal fluctuations given in the $N - S$ basis. We introduced $\Lambda_1 = \lambda_1 + \lambda_2/2$, $\Lambda_2 = \lambda_1 + \lambda_2$, $\Lambda_3 = \lambda_1 + 3\lambda_2/2$, $A = 3g_F^4/(64\pi^2)$, $C = 6g_F^2$, and following [7] $X = 1 + 4\ln \frac{g_F \phi_N}{2M_0}$ and $Y = 1 + 4\ln \frac{g_F \phi_S}{\sqrt{2}M_0}$, with M_0 being the renormalization scale. T_f , the thermal part of the tadpole integral, is defined in (42) and $B_f = -dT_f/(dm_f^2)$.

Tree-level meson squared masses	Fermionic vacuum correction	Fermionic thermal correction
$m_\pi^2 = Z_\pi^2(m_0^2 + \Lambda_1\phi_N^2 + \Lambda_1\phi_S^2 - c_1\phi_S/\sqrt{2})$	$\Delta m_\pi^2 = -AZ_\pi^2\phi_N^2X$	$\delta m_\pi^2 = CZ_\pi^2T_u$
$m_K^2 = Z_K^2[m_0^2 + \Lambda_1\phi_N^2 + \Lambda_2\phi_S^2 - (c_1 + \sqrt{2}\lambda_2\phi_S)\phi_N/2]$	$\Delta m_K^2 = -AZ_K^2\frac{\phi_N^3X + 2\sqrt{2}\phi_S^3Y}{\phi_N + \sqrt{2}\phi_S}$	$\delta m_K^2 = CZ_K^2\frac{\phi_N T_u + \sqrt{2}\phi_S T_s}{\phi_N + \sqrt{2}\phi_S}$
$m_{\eta_N}^2 = Z_{\eta_N}^2(m_0^2 + \Lambda_1\phi_N^2 + \Lambda_1\phi_S^2 + c_1\phi_S/\sqrt{2})$	$\Delta m_{\eta_N}^2 = -AZ_{\eta_N}^2\phi_N^2X$	$\delta m_{\eta_N}^2 = CZ_{\eta_N}^2T_u$
$m_{\eta_S}^2 = Z_{\eta_S}^2(m_0^2 + \Lambda_1\phi_N^2 + \Lambda_2\phi_S^2)$	$\Delta m_{\eta_S}^2 = -2AZ_{\eta_S}^2\phi_S^2Y$	$\delta m_{\eta_S}^2 = CZ_{\eta_S}^2T_s$
$m_{\eta_{NS}}^2 = Z_{\eta_N}Z_{\eta_S}c_1\phi_N/\sqrt{2}$	$\Delta m_{\eta_{NS}}^2 = 0$	$\delta m_{\eta_{NS}}^2 = 0$
$m_{a_0}^2 = m_0^2 + \Lambda_3\phi_N^2 + \Lambda_1\phi_S^2 + c_1\phi_S/\sqrt{2}$	$\Delta m_{a_0}^2 = -A\phi_N^2(4 + 3X)$	$\delta m_{a_0}^2 = C(T_u - \frac{g_F^2\phi_N^2}{2}B_u)$
$m_{K_0^*}^2 = Z_{K_0^*}^2[m_0^2 + \Lambda_1\phi_N^2 + \Lambda_2\phi_S^2 + (c_1 + \sqrt{2}\lambda_2\phi_S)\phi_N/2]$	$\Delta m_{K_0^*}^2 = -AZ_{K_0^*}^2\frac{\phi_N^3X - 2\sqrt{2}\phi_S^3Y}{\phi_N - \sqrt{2}\phi_S}$	$\delta m_{K_0^*}^2 = CZ_{K_0^*}^2\frac{\phi_N T_u - \sqrt{2}\phi_S T_s}{\phi_N - \sqrt{2}\phi_S}$
$m_{\sigma_N}^2 = m_0^2 + 3\Lambda_1\phi_N^2 + \Lambda_1\phi_S^2 - c_1\phi_S/\sqrt{2}$	$\Delta m_{\sigma_N}^2 = -A\phi_N^2(4 + 3X)$	$\delta m_{\sigma_N}^2 = C(T_u - \frac{g_F^2\phi_N^2}{2}B_u)$
$m_{\sigma_S}^2 = m_0^2 + \Lambda_1\phi_N^2 + 3\Lambda_2\phi_S^2$	$\Delta m_{\sigma_S}^2 = -2A\phi_S^2(4 + 3Y)$	$\delta m_{\sigma_S}^2 = C(T_s - \frac{g_F^2\phi_S^2}{2}B_s)$
$m_{\sigma_{NS}}^2 = 2\lambda_1\phi_N\phi_S - c_1\phi_N/\sqrt{2}$	$\Delta m_{\sigma_{NS}}^2 = 0$	$\delta m_{\sigma_{NS}}^2 = 0$

and thermal fluctuations, respectively. We note that the mesonic fields are set to their expectation value only after the differentiation is performed.

In the case of three flavors, $\delta m_{i,ab}^2$ was first calculated without the inclusion of the Polyakov loop in [6] and in the presence of the Polyakov loop in [34] at $\mu = 0$ and in [33] at $\mu \neq 0$, while $\Delta m_{i,ab}^2$ was first computed in [7]. We shall review below the expressions of $\Delta m_{i,ab}^2$ and $\delta m_{i,ab}^2$, and in Table I we explicitly give their contributions to the tree-level masses, which are also listed there. Note that in the $N - S$ basis there are no off-diagonal contributions to the curvature matrix coming from the fermionic fluctuations. In the respective mixing sector, the eigenvalues $m_{\eta'/\eta}^2$ and $m_{f_0^H/f_0^L}^2$ can be computed with the following formulas:

$$m_{\eta'/\eta}^2 = \frac{1}{2} \left[m_{\eta_N}^2 + m_{\eta_S}^2 \pm \sqrt{(m_{\eta_N}^2 - m_{\eta_S}^2)^2 + 4m_{\eta_{NS}}^4} \right], \quad (33)$$

$$m_{f_0^H/f_0^L}^2 = \frac{1}{2} \left[m_{\sigma_N}^2 + m_{\sigma_S}^2 \pm \sqrt{(m_{\sigma_N}^2 - m_{\sigma_S}^2)^2 + 4m_{\sigma_{NS}}^4} \right]. \quad (34)$$

The fermionic vacuum contribution to the curvature mass is given by

$$\begin{aligned} \Delta m_{i,ab}^2 &= \frac{\partial^2 \Omega_{qq}^{(0)v}}{\partial \varphi_{i,a} \partial \varphi_{i,b}} \Big|_{\min} \\ &= -\frac{3}{8\pi^2} \sum_{f=u,d,s} \left[\left(\frac{3}{2} + \log \frac{m_f^2}{M_0^2} \right) m_{f,a}^{2(i)} m_{f,b}^{2(i)} \right. \\ &\quad \left. + m_f^2 \left(\frac{1}{2} + \log \frac{m_f^2}{M_0^2} \right) m_{f,ab}^{2(i)} \right], \end{aligned} \quad (35)$$

where we introduced, as in [6], shorthands for the first and second derivatives of the constituent quark mass

squared with respect to the meson fields: $m_{f,a}^{2(i)} \equiv \partial m_f^2 / \partial \varphi_{i,a}$ and $m_{f,ab}^{2(i)} \equiv \partial^2 m_f^2 / \partial \varphi_{i,a} \partial \varphi_{i,b}$.

The correction to the curvature matrix due to the fermionic thermal fluctuations in the presence of the Polyakov loop reads

$$\begin{aligned} \delta m_{i,ab}^2 &= \frac{\partial^2 \Omega_{qq}^{(0)T}}{\partial \varphi_{i,a} \partial \varphi_{i,b}} \Big|_{\min} = 6 \sum_{f=u,d,s} \int \frac{d^3p}{(2\pi)^3} \frac{1}{2E_f(p)} \\ &\times \left[(f_f^+(p) + f_f^-(p)) \left(m_{f,ab}^{2(i)} - \frac{m_{f,a}^{2(i)} m_{f,b}^{2(i)}}{2E_f^2(p)} \right) \right. \\ &\quad \left. + (B_f^+(p) + B_f^-(p)) \frac{m_{f,a}^{2(i)} m_{f,b}^{2(i)}}{2TE_f(p)} \right], \end{aligned} \quad (36)$$

where

$$f_f^\pm(p) = \frac{\Phi^\pm e^{-\beta E_f^\pm(p)} + 2\Phi^\mp e^{-2\beta E_f^\pm(p)} + e^{-3\beta E_f^\pm(p)}}{g_f^\pm(p)}, \quad (37)$$

is the modified Fermi-Dirac distribution functions for quarks (+) and antiquarks (−) and, following Ref. [34], we also introduced $B_f^\pm(p) = 3(f_f^\pm(p))^2 - C_f^\pm(p)$ with

$$C_f^\pm(p) = \frac{\Phi^\pm e^{-\beta E_f^\pm(p)} + 4\Phi^\mp e^{-2\beta E_f^\pm(p)} + 3e^{-3\beta E_f^\pm(p)}}{g_f^\pm(p)}. \quad (38)$$

To obtain the mass squares, whose first and second derivatives appear in Eqs. (35) and (36), we have to find the eigenvalues of the square of the $\gamma_0 \mathcal{M}$ matrix from Eq. (21), which is a 12×12 matrix in the Dirac and flavor space, or, equivalently, of the matrix $\mathcal{N} \mathcal{N}^\dagger$, where $\mathcal{N} = \sigma_a \lambda_a + i\pi_a \lambda_a$, which is a 3×3 matrix. An easy way to do the calculation of a given derivative is to set to zero all the fluctuating fields not used in the differentiation. The calculation is straightforward and as noted in [6],

TABLE II. The first and second derivatives of the quark squared masses with respect to the scalar (S) and pseudoscalar (P) meson fields, evaluated in the $N - S$ basis at the extremum of the grand potential. All entries of the omitted $ab = NS$ rows are vanishing. The result holds in the isospin symmetric case and a summation over $l \in \{u, d\}$ is understood in the first two columns.

i	ab	$m_{l,a}^{2(i)} m_{l,b}^{2(i)} / g_F^4$	$m_{l,ab}^{2(i)} / g_F^2$	$m_{s,a}^{2(i)} m_{s,b}^{2(i)} / g_F^4$	$m_{s,ab}^{2(i)} / g_F^2$
S	11	$\frac{1}{2} \phi_N^2$	1	0	0
S	44	0	$\frac{Z_{K^*}^2 \phi_N}{\phi_N - \sqrt{2} \phi_S}$	0	$\frac{-\sqrt{2} Z_{K^*}^2 \phi_S}{\phi_N - \sqrt{2} \phi_S}$
S	NN	$\frac{1}{2} \phi_N^2$	1	0	0
S	SS	0	0	ϕ_S^2	1
P	11	0	Z_π^2	0	0
P	44	0	$\frac{Z_K^2 \phi_N}{\phi_N + \sqrt{2} \phi_S}$	0	$\frac{\sqrt{2} Z_K^2 \phi_S}{\phi_N + \sqrt{2} \phi_S}$
P	NN	0	$Z_{\eta_N}^2$	0	0
P	SS	0	0	0	$Z_{\eta_S}^2$

some cancellations occur in the isospin symmetric case, where the mass squared of the two light quarks can be combined. The result is given in the $N - S$ basis in Table II which, in the case of the $L\sigma M$, appeared first in the $0 - 8$ basis in [6].

For $\bar{\Phi} = \Phi = 1$, the distribution functions $f_f^\pm(p)$ goes over into the usual Fermi-Dirac distributions for quarks and antiquarks, $f_f^\pm(p) \rightarrow f_{f,\text{FD}}^\pm(p) = 1/(e^{\beta(E_f(p) \mp \mu_f)} + 1)$. In this limit, which is expected to be reached at high temperature, $B_f^\pm(p) \rightarrow -f_{f,\text{FD}}^\pm(p)(1 - f_{f,\text{FD}}^\pm(p))$, and one recovers the expression of Ref. [6] for the curvature mass, obtained in the linear sigma model without the inclusion of the Polyakov loop. When $\bar{\Phi} = \Phi = 0$, which is reached for vanishing temperature, the so-called “statistical confinement” occurs, as $f_f^\pm(p) \rightarrow 1/(e^{\beta(3E_f(p) \mp \mu_f)} + 1)$, which means that at small temperature three quark states, that is excitations with zero triality, represent the effective degrees of freedom [21].

C. Field equations

Up to this point we were quite formal in dealing with the consequence of the quark’s propagation on a constant gluon background field in the temporal direction. Now we have to face the situation that, since Φ and $\bar{\Phi}$ are

complex, the grand potential we arrived at is, in fact, a complex function of complex variables. It is easy to see that $\Omega_{\bar{q}q}^{(0)\text{T}}(T, \mu_q)$ in (24) has an imaginary part for $\mu_q \neq 0$, which is the manifestation of the sign problem in the present context, and the question is how to extract physical information from the grand potential (see also the discussion in [35]). In the mean-field approximation of Ref. [22] (see also [36]) the traced Polyakov loops Φ and $\bar{\Phi}$ introduced in (12) are replaced by their thermal expectation values $\langle \Phi \rangle$ and $\langle \bar{\Phi} \rangle$, that is by the Polyakov loop variables, which at $\mu_B \neq 0$ are treated as two real and independent quantities (at $\mu_B = 0$ they are equal). Adopting this approach and using for simplicity the notation Φ and $\bar{\Phi}$ for the Polyakov loop variable, it is understood that from now on in Eqs. (28), (37), and (38) the fields Φ and $\bar{\Phi}$ are real and independent. In this approach the grand potential Ω is real and the physical point (extremum of Ω) is a saddle point. Working with real Polyakov loop variables Φ and $\bar{\Phi}$ seems to be supported by the study performed in the massive extension of the Landau-DeWitt gauge, where the self-consistent gauge fixing condition imposes constraints on the background gauge fields \bar{A}^3 and \bar{A}^8 [which correspond to ϕ_3 and ϕ_8 of (13)]. As the study in [37] reveals, for real values of μ_B the constraints are obeyed by real \bar{A}^3 and imaginary \bar{A}^8 gauge fields, and these field configurations correspond to real and independent Polyakov loop variables Φ and $\bar{\Phi}$.³ We mention that in some cases, another approach is preferred in the $PL\sigma M$, in which the imaginary part of the potential is neglected [35]. In this case the physical point is a minimum, which makes possible the investigation of the nucleation occurring during a first order phase transition, but has the drawback that the difference between the expectation values of the traced Polyakov loop and its conjugate vanishes at $\mu_B \neq 0$.

In view of the above discussion, the field equations, which determine the dependence on T and $\mu_B = 3\mu_q$ of the chiral condensates ϕ_N and ϕ_S and the Polyakov loop variables Φ and $\bar{\Phi}$, are obtained by extremizing the grand potential,

$$\frac{\partial \Omega_H}{\partial \phi_N} = \frac{\partial \Omega_H}{\partial \phi_S} = \frac{\partial \Omega_H}{\partial \Phi} = \frac{\partial \Omega_H}{\partial \bar{\Phi}} = 0. \quad (39)$$

In our hybrid approach we include in the field equations only the vacuum and thermal fluctuations of the constituent quarks and leave out the corresponding mesonic fluctuations. In this case, the explicit field equations read

$$-\frac{d}{d\Phi} \left(\frac{U(\Phi, \bar{\Phi})}{T^4} \right) + \frac{6}{T^3} \sum_{f=u,d,s} \int \frac{d^3 p}{(2\pi)^3} \left(\frac{e^{-\beta E_f^-(p)}}{g_f^-(p)} + \frac{e^{-2\beta E_f^+(p)}}{g_f^+(p)} \right) = 0, \quad (40a)$$

³ We thank Urko Reinosa for explaining to us the relevance of his works in the present context and for sharing with us the ideas and

subtleties related to the construction of a physically meaningful potential.

$$-\frac{d}{d\bar{\Phi}}\left(\frac{U(\Phi, \bar{\Phi})}{T^4}\right) + \frac{6}{T^3} \sum_{f=u,d,s} \int \frac{d^3p}{(2\pi)^3} \left(\frac{e^{-\beta E_f^+(p)}}{g_f^+(p)} + \frac{e^{-2\beta E_f^-(p)}}{g_f^-(p)} \right) = 0, \quad (40b)$$

$$m_0^2 \phi_N + \left(\lambda_1 + \frac{1}{2} \lambda_2 \right) \phi_N^3 + \lambda_1 \phi_N \phi_S^2 - \frac{1}{\sqrt{2}} c_1 \phi_N \phi_S - h_{0N} + \frac{3}{2} g_F (\langle \bar{q}_u q_u \rangle_T + \langle \bar{q}_d q_d \rangle_T) = 0, \quad (40c)$$

$$m_0^2 \phi_S + (\lambda_1 + \lambda_2) \phi_S^3 + \lambda_1 \phi_N^2 \phi_S - \frac{\sqrt{2}}{4} c_1 \phi_N^2 - h_{0S} + \frac{3}{\sqrt{2}} g_F \langle \bar{q}_s q_s \rangle_T = 0, \quad (40d)$$

where $U(\Phi, \bar{\Phi})$ is the Polyakov loop potential (15) and, by matching the renormalization of the effective potential done in Sec. III A, we defined the renormalized expectation value⁴ as

$$\langle \bar{q}_f q_f \rangle_T = 4m_f \left[-\frac{m_f^2}{16\pi^2} \left(\frac{1}{2} + \ln \frac{m_f^2}{M_0^2} \right) + T_f \right], \quad (41)$$

with the thermal part of the fermion tadpole integral given by

$$T_f = \int \frac{d^3p}{(2\pi)^3} \frac{1}{2E_f(p)} (f_f^-(p) + f_f^+(p)). \quad (42)$$

IV. DETERMINATION OF THE MODEL PARAMETERS

There are altogether 16 unknown parameters, 15 parameters found in the Lagrangian given in Eq. (1) and the renormalization scale M_0 (see Sec. III A). For the renormalization scale we choose three different initial values, namely $M_0 = 0.3, 0.9, 1.5$ GeV and run the parametrization for them. After finding a good solution—which includes a particular M_0 value—we take it as an initial condition and minimize for M_0 around that solution. From the remaining 15 Lagrangian parameters δ_N can be incorporated (without loss of generality) into m_1 —the bare (axial)vector mass, while the external fields h_{0N} and h_{0S} are replaced by the scalar condensates ϕ_N and ϕ_S with the help of the field equations (40c) and (40d) at zero temperature. Consequently, there are 14 parameters left to be determined, which are the following: the bare (pseudo)scalar mass m_0 ; the (pseudo)scalar self-couplings λ_1 and λ_2 ; the $U_A(1)$ anomaly coupling c_1 ; the bare (axial)vector mass m_1 ; the (axial)vector–(pseudo)scalar couplings h_1 , h_2 and h_3 ; the external field δ_S which explicitly breaks the chiral symmetry in the (axial)vector sector; the scalar condensates ϕ_N and ϕ_S ; the Yukawa coupling g_F ; and two (axial)vector couplings g_1 and g_2 .

In the parametrization procedure we use alongside 29 vacuum quantities, that is 15 masses, 12 tree-level decay widths, 2 Partially Conserved Axialvector Current (PCAC) relations $f_\pi = \phi_N/Z_\pi$ and $f_K = (\phi_N + \sqrt{2}\phi_S)/(2Z_K)$, and also the pseudocritical temperature T_c (see the next paragraph for explanation). The masses used are the following: the curvature masses of the pseudoscalars m_π , m_K , m_η , $m_{\eta'}$ and the scalars m_{a_0} , $m_{K_0^*}$, $m_{f_0^L}$, $m_{f_0^H}$ listed in Table I, where the fermionic corrections to the tree-level masses are also given [see also Eqs. (33) and (34)]; the tree-level masses of the vector mesons $m_\rho = m_\omega$, m_{K^*} , m_Φ , the axial vector mesons $m_{a_1} = m_{f_1^L}$, $m_{f_1^H}$ to be found in [1]; the tree-level constituent quark masses $m_{u,d}$, m_s given in (25).⁵ The decay widths used are the vector decays $\Gamma_{\rho \rightarrow \pi\pi}$, $\Gamma_{K^* \rightarrow K\pi}$, $\Gamma_{\Phi \rightarrow KK}$, the axial vector decays $\Gamma_{a_1 \rightarrow \rho\pi}$, $\Gamma_{a_1 \rightarrow \pi\gamma}$, $\Gamma_{f_1 \rightarrow K^*K}$, and the scalar decays Γ_{a_0} , $\Gamma_{K_0^*}$, $\Gamma_{f_0^L \rightarrow \pi\pi}$, $\Gamma_{f_0^L \rightarrow KK}$, $\Gamma_{f_0^H \rightarrow \pi\pi}$, $\Gamma_{f_0^H \rightarrow KK}$ given in [1] and Appendix A. The value of the masses and decay constants are compared with the corresponding experimental value taken from the PDG [2] through the χ^2 minimization method of Ref. [38] similarly as in [1], but with some important differences listed below. One such difference, mentioned already and detailed more latter, is the inclusion of the pseudocritical temperature T_c in the minimization process. We take the mean value given in the PDG (in case of charged particles, the neutral and charged masses are averaged) and for the error we allow for a 20% variation with respect to the PDG value for the masses and decay widths of the scalar sector, 10% for the constituent quark masses and 5% for all the other quantities. We use this large error in case of the scalars mainly because they mix with each other and our fields do not correspond to pure physical particles, while in case of the constituent quarks, their dynamically generated mass depends on how it is defined and calculated. All other errors of the masses and decay widths of the pseudoscalars, vectors and axial vectors are much smaller experimentally; however, we used 5% for them due to model limitations and approximations (e.g., isospin symmetry). All the data used for the parametrization are listed in Appendix B.

⁴ It is worth noting that the expectation value $\langle \bar{q}_f q_f \rangle$ is calculated within the framework of the present model containing constituent quarks and it is not directly related to $\langle \bar{q}q \rangle$ appearing in the QCD.

⁵ Note that the relations $m_\rho = m_\omega$ and $m_{a_1} = m_{f_1^L}$ hold at tree level in our model and that we do not use m_{K_1} . For the latter see the discussion in [1].

Compared to [1], the modifications in the parametrization of the model are the following.

- (i) Since here we use a different anomaly term [see (1)], the terms proportional to c_1 are different in the expressions of the tree-level pseudo(scalar) masses and the scalar decay widths, which are listed explicitly in the first column of Table I and in Appendix A, respectively. The expressions of the (axial)vector meson masses and decay widths are unchanged.
- (ii) A small modification in the present case is that for the $a_0(980)$ particle we fit to the value of the total width found in [2], instead of fitting to the value of the two amplitudes $|\mathcal{M}_{a_0(980) \rightarrow KK}|$ and $|\mathcal{M}_{a_0(980) \rightarrow \eta\pi}|$ found in [39].
- (iii) We now include the f_0 masses and decay widths into the global fit, as opposed to [1], where we first did a global fit without using the properties of the f_0 mesons and only after that we analyzed the consequences of the fit on the f_0 's.
- (iv) We consider here the effects of the fermion vacuum fluctuations, case in which the expression of the (pseudo)scalar masses are modified, as shown in the second column of Table I.
- (v) Working in the isospin symmetric limit, we use now the two additional tree-level equations for the constituent quark masses given in (25). Their explicit expression contains the Yukawa coupling g_F and the values $m_{u,d} = 308$ MeV and $m_s = 483$ MeV were used for the fit. These values are obtained from a nonrelativistic mass formula for the light mesons in which spin-spin interaction is taken into account, as presented in Chap. 5.5 of Ref. [40].

As was discussed in [1], the scalar sector below 2 GeV contains more physical particles than states in one $q\bar{q}$ nonet (consisting of a_0 , K_0^* , f_0^L , f_0^H), since in nature there are two a_0 , two K_0^* , and five f_0 particles in the considered energy range. These particles are the $a_0(980)$ and $a_0(1450)$, which will be denoted by a_0^1 and a_0^2 ; the $K_0^*(800)$ and $K_0^*(1430)$, which will be denoted by K_0^{*1} and K_0^{*2} ; and the $f_0(500)$ [previously called as σ or $f_0(600)$], $f_0(980)$, $f_0(1370)$, $f_0(1500)$, and $f_0(1710)$, which will be denoted by f_0^1, \dots, f_0^5 , respectively. Consequently, there are 40 possibilities to assign the existing scalar physical particles to the corresponding scalar nonet states.

Since compared to [1] our parametrization considerably changed due to the inclusion of the f_0 masses, decay widths, and fermionic vacuum fluctuations, we reran the fitting procedure for all 40 cases and for every M_0 value mentioned earlier and retained only those solutions of the χ^2 minimization, which gave the lowest χ^2 values. However, by using only zero temperature quantities (PCAC relations, masses and decay widths) in the parametrization we would end up with lots of possible

solutions with very close χ^2 values, which could produce various, even physically unacceptable, thermodynamical behaviors. More specifically, the T_c pseudocritical temperature at zero baryon chemical potential, which should be around 150 MeV,⁶ can reach very high values ($\gtrsim 350$ MeV) in case of some solutions. Thus we chose to include the physical value of T_c in the parametrization with a 10% error. Additionally, we only considered solutions that had $T_c < 180$ MeV. For the determination of the T_c we solved the four coupled field equations Eqs. (40a)-(40d) at $\mu_B = 0$ and defined T_c as the temperature for which the value of the so-called subtracted chiral condensate is 0.5. This quantity, defined in [43] as

$$\Delta_{l,s}(T) = \frac{(\phi_N - \frac{h_{0N}}{h_{0S}}\phi_S)|_T}{(\phi_N - \frac{h_{0N}}{h_{0S}}\phi_S)|_{T=0}}, \quad (43)$$

can be measured on the lattice, and it takes values between 0 and 1.

The χ^2 and $\chi_{\text{red}}^2 \equiv \chi^2/N_{\text{dof}}$ values⁷ for the first ten best solutions are shown in Table III along with the corresponding particle assignments. Interestingly, in the case of the ten best solutions the value of M_0 was always 0.3 GeV (from the three possibilities 0.3, 0.9, and 1.5 GeV). In these solutions we used the logarithmic Polyakov loop potential (15) with $T_0 = 182$ MeV. Considering that we would like to carry out the thermodynamical analysis with one particular set of parameters (which means one particular assignment of the scalar states), we could simply choose the first one. However, since the first couple of solutions are not very far from each other in χ^2 values, it is better if we take a closer look at the details of the fits and see how well they describe the spectrum physically. The detailed fit results of the first two best solutions are shown in Table V of Appendix B together with the result taken from [1]. In the case of the two best solutions the majority of the 30 physical quantities listed there are in good agreement with the experimental values. However, there are some quantities that are not well described, like the mass of a_1 , which we find in any current fit smaller than its experimental value, and which consequently result in too small values for the a_1 decays as well. Considering the first assignment $a_0^1 K_0^{*1} f_0^1 f_0^2$ we cannot see any inconsistency; on the other hand, in case of the second assignment (right “Fit” column), $a_0^1 K_0^{*1} f_0^1 f_0^3$, the f_0^H should correspond to $f_0(1370)$, while the fitted values of its mass and $\Gamma_{f_0^H \rightarrow KK}$ decay—which are 802.4 MeV and 0 MeV, respectively—are much closer to the data of $f_0(980)$ ($\equiv f_0^2$). Though its other decay turns out to be $\Gamma_{f_0^H \rightarrow \pi\pi} = 249.5$ MeV, this

⁶ Continuum extrapolated lattice results give $T_c = 151$ MeV from the peak of the chiral susceptibility [41] and $T_c = 157$ MeV if the inflection point of the subtracted chiral condensate is used [42].

⁷ The number of the degrees of freedom, N_{dof} is the difference between the number of fitted quantities (30) and the number of fitting parameters (14). Note that M_0 is kept fixed.

TABLE III. χ^2 and $\chi_{\text{red}}^2 = \chi^2/N_{\text{dof}}$ values ($N_{\text{dof}} = 16$, because M_0 is kept fixed) for the first ten best solutions of the fit together with the corresponding physical scalar meson particle assignment. See the text for the meaning of the superscript in the particle assignment.

Particle assignment	χ^2	χ_{red}^2
$a_0^1 K_0^{*1} f_0^1 f_0^2$	18.57	1.16
$a_0^1 K_0^{*1} f_0^1 f_0^3$	21.38	1.34
$a_0^1 K_0^{*2} f_0^1 f_0^3$	27.80	1.74
$a_0^1 K_0^{*2} f_0^1 f_0^2$	28.42	1.77
$a_0^1 K_0^{*1} f_0^2 f_0^3$	29.37	1.83
$a_0^2 K_0^{*1} f_0^1 f_0^2$	31.65	1.98
$a_0^2 K_0^{*1} f_0^1 f_0^3$	33.41	2.09
$a_0^1 K_0^{*2} f_0^2 f_0^3$	35.99	2.25
$a_0^1 K_0^{*1} f_0^1 f_0^5$	38.87	2.43
$a_0^2 K_0^{*1} f_0^2 f_0^3$	41.54	2.60

value indeed belongs to $f_0(1370)$. This means that this assignment can be excluded even on the grounds of physical inconsistency. With the same argument all elements of the list in Table III can be excluded except one, which is indeed the best solution with assignment $a_0^1 K_0^{*1} f_0^1 f_0^2$ (middle “Fit” column). Thus we choose the parameter set belonging to the $a_0^1 K_0^{*1} f_0^1 f_0^2$ assignment for the thermodynamical investigations of the next section and minimize for M_0 , which reduces the χ^2 slightly to 18.53. The corresponding values of the parameters are given in Table IV. Using Eqs. (40c) and (40d) at $T = 0$ one obtains for the value of the external fields $h_{0N} = (108.488 \text{ MeV})^3$ and $h_{0S} = (287.832 \text{ MeV})^3$.

It is worth noting that according to [1] without fitting the $f_0^{L/H}$ mesons the best solution is the combination $a_0^2 K_0^{*2}$, and we argued that with that solution the most favorable $f_0^{L/H}$ assignment is the $f_0^{3/5}$. For a general investigation the procedure followed in [1] is the right strategy, since the physically observed f_0 states are probably mixtures of elementary diquark, tetraquark and glueball states (from which the latter ones are not included in the present model); therefore, our $f_0^{L/H}$ states cannot be identified directly with any of the f_0^i states. Since we could not quantify that mixing, we left out the f_0 's from the fit. However, in this study, the thermodynamical properties of the system depend on f_0^L very strongly, and thus we had to identify it with one of the f_0^i states and include it in the parametrization.

V. RESULTS

In this section we present the dependence on the temperature and chemical potential of various physical quantities determined with the best set of parameters found with our parametrization procedure. We compare the variation of the condensates and that of the pressure and

TABLE IV. Parameter values in the case of the $a_0^1 K_0^{*1} f_0^1 f_0^2$ particle assignment obtained using the logarithmic Polyakov loop potential (15) with $T_0 = 182 \text{ MeV}$.

Parameter	Value	Parameter	Value
ϕ_N [GeV]	0.1411	g_1	5.6156
ϕ_S [GeV]	0.1416	g_2	3.0467
m_0^2 [GeV ²]	2.3925_{E-4}	h_1	27.4617
m_1^2 [GeV ²]	6.3298_{E-8}	h_2	4.2281
λ_1	-1.6738	h_3	5.9839
λ_2	23.5078	g_F	4.5708
c_1 [GeV]	1.3086	M_0 [GeV]	0.3511
δ_S [GeV ²]	0.1133		

the quantities derived from it, like the energy density, the interaction measure, and the speed of sound, with recent continuum extrapolated lattice results. In doing so, we vary the parameter T_c^{glue} of the improved Polyakov loop potential (17) in the range of [182, 270] MeV, in an attempt to see whether the lattice result could restrict its value. Changing T_c^{glue} affects the value of T_c , but it does not affect the vacuum value of the quantities used for parametrization. We also study the $\mu_B - T$ phase diagram and the existence of the CEP.

A. Temperature variation of condensates and meson masses at $\mu_B = 0$

In Fig. 1 we study at $\mu_B = 0$ the temperature variation of the nonstrange and strange chiral condensates, Polyakov loop expectation value, scalar and pseudoscalar curvature masses and the corresponding mixing angles. These results are obtained using the improved Polyakov loop potential U_{glue} of Eq. (17) with $T_c^{\text{glue}} = 182 \text{ MeV}$,⁸ as the value of the critical glue temperature. We see that the chiral condensates stay close to their vacuum values up to some quite high value of the temperature of order 100 MeV. This is the usual manifestation of the so-called “Polyakov cooling mechanism” [44] already observed in [45], namely, that when the Polyakov loop is coupled to chiral quarks, any quark observable at small temperature (deep in the hadronic phase) takes a value obtained in the theory without the Polyakov loop at a lower temperature, of the order T/N_c . When the values of the condensates start to drop, a bumpy behavior can be observed in both the strange and nonstrange condensates. This behavior, clearly shown by the temperature derivative of the condensates, is reflected by the temperature evolution of the masses.

Next, let us consider the restoration of chiral symmetry from the parity doubling perspective [46], that is, by

⁸ For other values of T_c^{glue} in the [182, 270] MeV interval the curves show a very similar behavior.

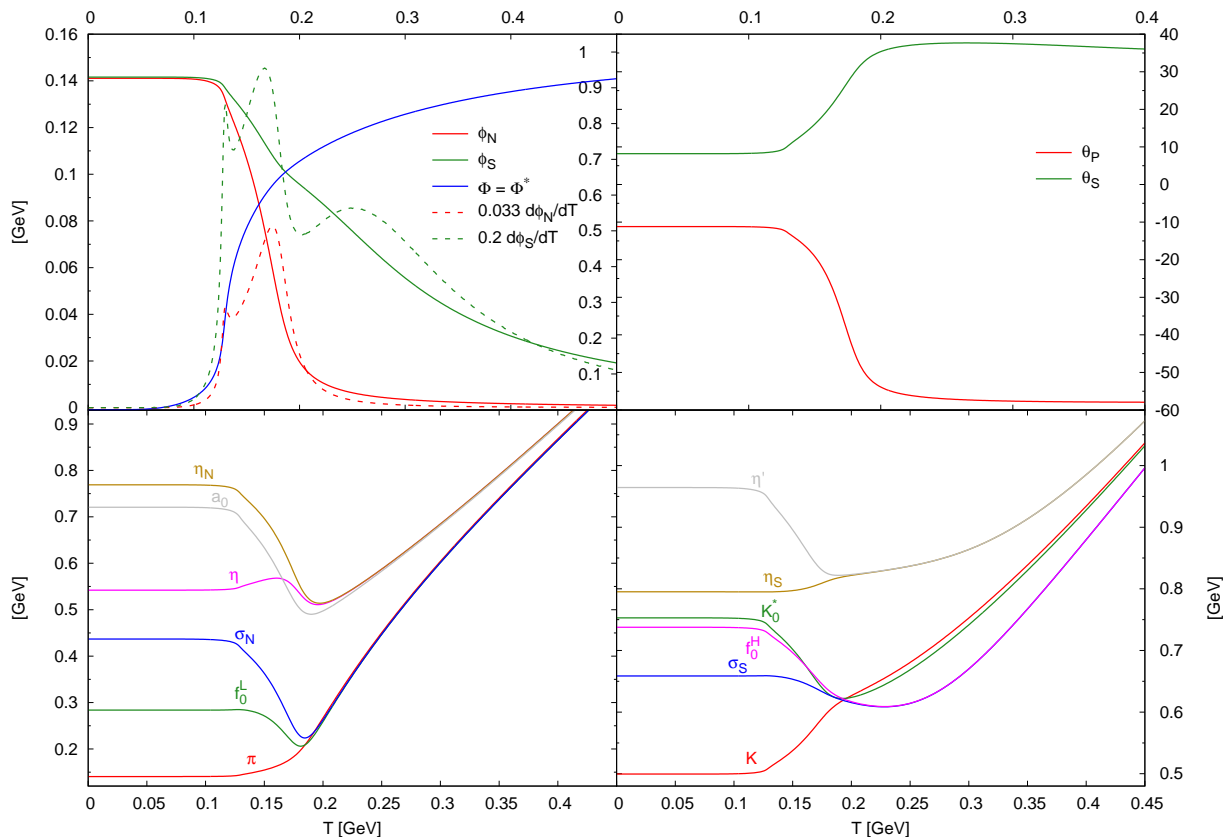


FIG. 1. Temperature dependence of various quantities obtained at $\mu_B = 0$ from the improved Polyakov loop potential U_{glue} (17) proposed in [28] (here we used $T_c^{\text{glue}} = 182$ MeV). Top left: nonstrange and strange chiral condensates along with their temperature derivative and the Polyakov loop expectation value; top right: scalar and pseudoscalar mixing angles; and bottom left and right: scalar and pseudoscalar curvature masses arranged according to chiral partners (π, f_0^L) , (η, a_0) and (K, K_0^*) , (η', f_0^H) , respectively. We also show the masses of the strange and nonstrange components of the two mixing sectors.

checking the mass degeneracy of a scalar meson with its opposite-parity partner. We see in Fig. 1 that in the nonstrange sector the $SU(2)$ chiral partners (π, f_0^L) and (η, a_0) become degenerate at $T \simeq 190$ MeV, which is slightly above the inflection point ($T_c = 172$ MeV) of the nonstrange condensate $\phi_N(T)$ and subtracted chiral condensate $\Delta_{l,s}(T)$. In the strange sector the chiral symmetry is restored at a much higher temperature, as there is a temperature range of around 200 MeV where the masses of the chiral partners (K, K_0^*) are close, but they only become degenerate above $T \simeq 450$ MeV. The masses of the η' and f_0^H approach each other, but they never become degenerate. This is the consequence of the fact that our anomaly parameter c_1 is temperature independent, and therefore the $U(1)_A$ symmetry is not restored in the explored temperature region. The nonrestoration of the $U(1)_A$ symmetry is visible also in the nonstrange sector, where the axial partners (π, a_0) and (η, f_0^L) do not become degenerate. We refer to the literature for the case when a temperature-dependent anomaly parameter is considered by using lattice results for the topological susceptibility. Typically, following Ref. [47], an anomaly parameter which decreases exponentially with

the temperature or density is considered, which results in a faster restoration of the chiral symmetry and an effective restoration of the $U(1)_A$ symmetry [46, 48].

We turn now to the scalar and pseudoscalar mixing angles in relation with the masses of the $f_0^L - f_0^H$ and $\eta - \eta'$ complexes. The big difference compared to previous results obtained by computing the grand potential with the same approximation we use here, but without the inclusion of the (axial)vector mesons, is that in our case, for temperatures below 0.9 GeV, one has $m_{f_0^L} \leq m_{\sigma_N} < m_{\sigma_S} \leq m_{f_0^H}$ and similarly $m_\eta \leq m_{\eta_N} < m_{\eta_S} \leq m_{\eta'}$ in contrast to previous studies, where $m_{\eta_N} > m_{\eta_S}$ and $m_{\sigma_N} > m_{\sigma_S}$ (see, e.g., [6]). The temperature evolution of both mixing angles is such that the situation of ideal flavor mixing is achieved at temperatures which are 2–3 times larger than T_c ; that is, f_0^L and η mesons are pure nonstrange $\bar{q}q$ states, while f_0^H and η' are pure strange ones.

Now we look more closely at the thermal evolution of the subtracted chiral condensate $\Delta_{l,s}$ given in (43) and investigate, as in Ref. [28], whether by comparing to the lattice result it is possible to restrict the values of some parameters of the improved Polyakov loop potential. We

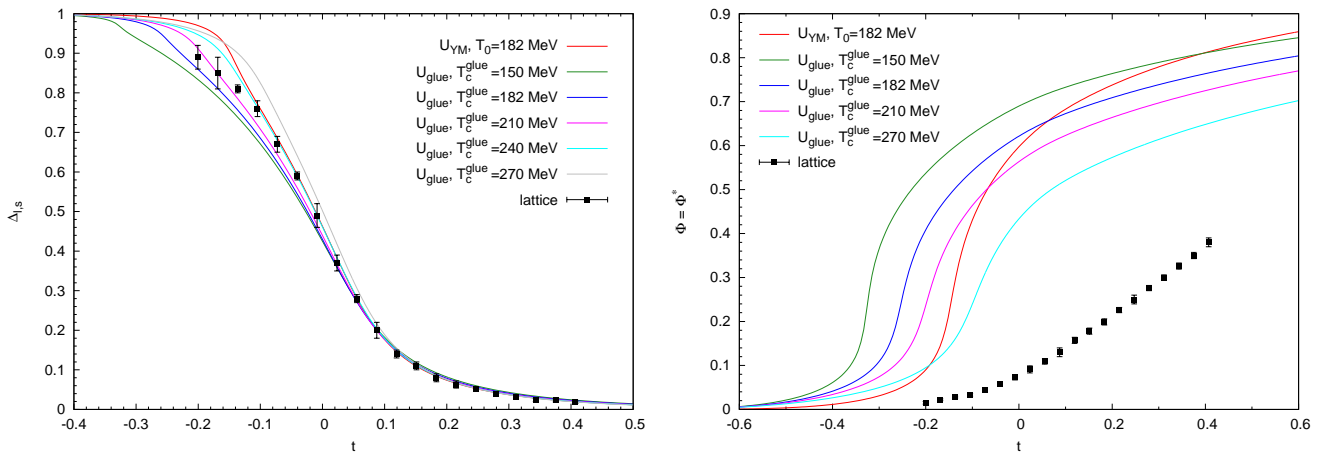


FIG. 2. The subtracted chiral condensate $\Delta_{l,s}$ given in (43) (left panel) and the Polyakov-loop expectation values (right panel) determined at $\mu_B = 0$ as a function of the reduced temperature $t = T/T_c - 1$ for different parametrizations of the Polyakov loop potential. We compare to the continuum extrapolated lattice result of the Wuppertal-Budapest Collaboration [42].

have already seen that our pseudocritical temperature is higher than the continuum extrapolated lattice result; therefore, we plot $\Delta_{l,s}$ as a function of the reduced temperature $t = T/T_c - 1$. To be able to compare with the lattice results of Ref. [42], we have to assure that we use the same definition for the pseudocritical temperature. During the parametrization we used, as a reasonable and numerically easy to implement approximation for T_c , the value of the temperature where $\Delta_{l,s} = 0.5$. Now we define T_c as the inflection point of $\Delta_{l,s}$ obtained by fitting $f(T) = a + b \arctan(c(\pi - dT))$ to our and the lattice results.⁹ Then, the value of the pseudocritical temperature is given by $T_c = \pi/d$. Fitting the above function to the lattice data in the range $T \in [145, 165]$ MeV we obtain $T_c = 156.35$ MeV, which is compatible with the reported value $157(3)(3)$. In our case, regarding the logarithmic Polyakov loop potential with $T_0 = 182$ MeV we obtain $T_c = 172$ MeV, and with the improved Polyakov loop potential we get $T_c \in (168, 189)$ MeV, depending on the T_c^{glue} value used.

In Fig. 2 we compare to lattice results the subtracted chiral condensate (43) obtained by using the original Polyakov loop potential with the transition temperature $T_0 = 182$ MeV and with the improved Polyakov loop potential with various values of the transition temperature T_c^{glue} . In agreement with the findings of Ref. [28], one observes that the chiral transition is slightly smoother when the improved Polyakov loop potential is used. The trend of the lattice results is well reproduced above T_c , where the difference between our results obtained with various Polyakov loop potentials is the smallest. Comparison with the lattice results at small values seems to favor

the improved Polyakov loop potential with a large value of the T_c^{glue} parameter in the range between 210 MeV and 240 MeV. In contrast with the nice agreement of the subtracted chiral condensate with the corresponding lattice result, the thermal evolution of the Polyakov loop expectation value shown in Fig. 2 is quite far from its lattice counterpart, as was also the case in Ref. [28]. The transition shown by the lattice result is much smoother, and although, as explained in Ref. [28], the use of the improved Polyakov loop potential makes the transition smoother compared to the case when the original logarithmic potential is used, the discrepancy from the lattice results remains significant. It was argued in [50] that, as the Polyakov loop requires renormalization, a temperature dependent rescaling has to be applied to the Polyakov loop expectation value calculated in an effective model when comparing it to the lattice value. With this idea the lattice result of two-color QCD was reproduced in a PNJL model. Because of the big discrepancy with the lattice data, we could not apply it in our case, where it seems that the mean field approximation is rather crude, as far as the expectation value of the Polyakov loop is concerned.

B. Thermodynamical quantities at $\mu_B = 0$

In this subsection we present the thermodynamical quantities derived from the pressure and compare them to the corresponding continuum extrapolated lattice results of Ref. [51]. The pressure is obtained from the grand potential defined in (19) as

$$p(T, \mu_q) = \Omega_H(T = 0, \mu_q) - \Omega_H(T, \mu_q). \quad (44)$$

Based on the pressure, one can compute thermodynamical observables like the entropy density $s = \partial p / \partial T$, the quark number density $\rho_q = \partial p / \partial \mu_q$, the quark num-

⁹ This procedure, used in [49] in the context of the $O(N)$ model, is accurate in the present context only if the temperature is restricted to a narrow range around the inflection point.

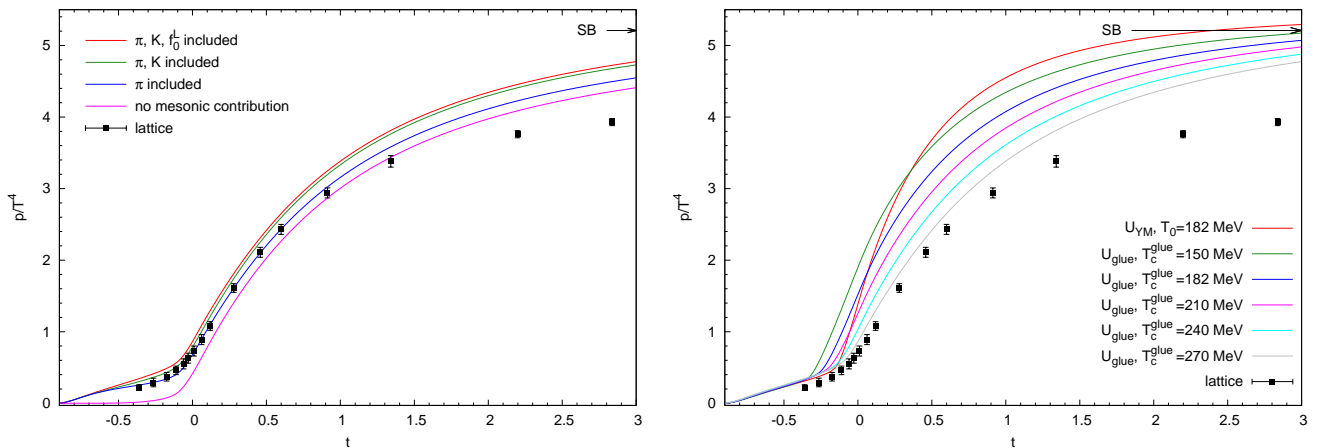


FIG. 3. The normalized pressure as a function of the reduced temperature $t = T/T_c - 1$ and its dependence on the inclusion of various mesonic thermal fluctuations in the case when the Polyakov loop potential U_{glue} is used with $T_c^{\text{glue}} = 270$ MeV (left panel) and on the various parametrizations of the Polyakov loop potential in the case when the contributions of π , K , and f_0^L are included (right panel). We compare to the continuum extrapolated lattice result of Ref. [51]. The arrow indicates the Stefan-Boltzmann limit of the QCD: $p_{\text{SB}}/T^4 = 5.209$.

ber susceptibility $\chi_q = \partial^2 p / \partial \mu_q^2$, the energy density $\epsilon = -p + Ts + \mu_q \rho_q$, as well as the scaled interaction measure $\Delta = (\epsilon - 3p)/T^4$ and the square of the speed of sound defined at $\mu_q = 0$ as $c_s^2 = dp/d\epsilon = s/(T(\partial s/\partial T))$.

So far we have not included any mesonic fluctuations in the grand potential, and consequently we solved the field equations without taking them into account. However, the contribution of the pions has to be included in the pressure, as at small temperature their mass is the smallest among all constituents of the model. In fact, it is known from textbooks that for small temperature the scaled pressure behaves as $p/T^4 \sim (m_\pi/T)^{3/2} \exp(-m_\pi/T)$. With the curvature mass determined according to Eq. (32) from a grand potential not containing mesonic fluctuations, the additive partial contribution of a meson $b \in \{\pi, K, f_0^L\}$ to the pressure is taken into account with the formula

$$\Delta p_b(T) = -n_b T \int \frac{d^3 p}{(2\pi)^3} \ln(1 - e^{-\beta E_b(p)}), \quad (45)$$

where $E_b(p) = \sqrt{p^2 + m_b^2}$, with m_b being the meson mass, and n_b is the meson multiplicity ($n_\pi = 3$, $n_K = 4$, and $n_{f_0^L} = 1$). Note that the fermion contribution to the pressure is included using Eq. (27).

In the left panel of Fig. 3 we see that the constituent quarks and the Polyakov loop potential give the major part of the contribution to the pressure around and beyond T_c and that at small temperature the pressure is pion dominated. Any additional mesonic contribution increases the pressure, and we see that with the inclusion of K and f_0^L , the pressure overshoots the lattice data. The contribution of the kaons is significant around T_c , while that of f_0^L is quite small in the entire temperature region. This has to do with the multiplicity of the kaons, as $n_K = 4n_{f_0^L}$. We included the contribution of f_0^L in the

pressure because in our approximation it is rather light in the vacuum and its mass decreases with the temperature roughly up to the pseudocritical temperature T_c .

In the right panel of Fig. 3 one observes that with the improved Polyakov loop potential the temperature increase of the pressure is smoother than with the original Polyakov loop potential (U_{YM}), where the Stefan-Boltzmann (SB) limit of the QCD (ideal gas of massless fermions and gluons) is reached already for $T \approx 1.5T_c$. One also observes that the overshooting of the pressure compared with the lattice data, when additional mesonic contributions are included beyond that of the pions, can be compensated to some degree by increasing the value of T_c^{glue} in the improved Polyakov loop potential. In the case of the pressure, we get close to the lattice data by using the maximal value $T_c^{\text{glue}} = 270$ MeV. This means that one cannot reproduce equally well all thermodynamical quantities with the same set of model parameters, as the value for which $\Delta_{l,s}$ is the closest to the lattice data is—according to Fig. 1—in the range $T_c^{\text{glue}} \in (210, 240)$ MeV. This inconsistency could be related to the inconsistent treatment of the mesonic contributions which are not included in the field equations when the model is solved. It is seen in general that the inclusion of mesonic fluctuations smoothes the chiral phase transition [52, 53], and therefore with their consistent inclusion we would expect a better agreement of the pressure and the derived thermodynamical quantities with the lattice results.

Some thermodynamical quantities derived from the pressure, like the scale interaction measure Δ , the square of the speed of sound c_s^2 , and the equation of state parameter p/ϵ (pressure over energy density), are presented in Figs. 4, 5, and 6. With the original Polyakov loop potential the maximum of the scaled interaction measure $\Delta(t)$ in Fig. 4 and the minimum of the square of the speed of

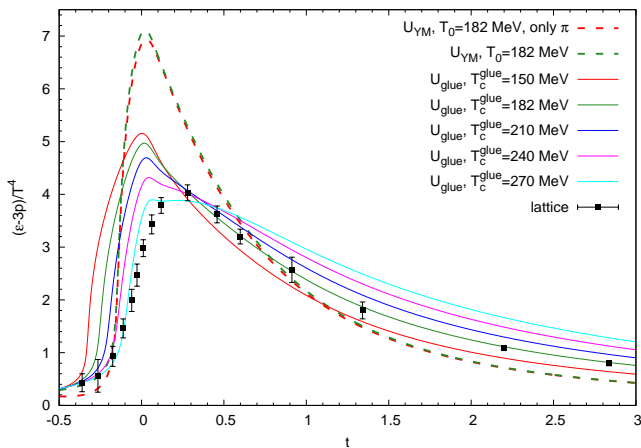


FIG. 4. The scaled interaction measure $\Delta = (\epsilon - 3p)/T^4$ as a function of $t = T/T_c - 1$ for various parametrizations of the Polyakov loop potential. Unless indicated otherwise, the contribution of π , K , and f_0^L is taken into account in the grand potential. The lattice result is from Ref. [51].

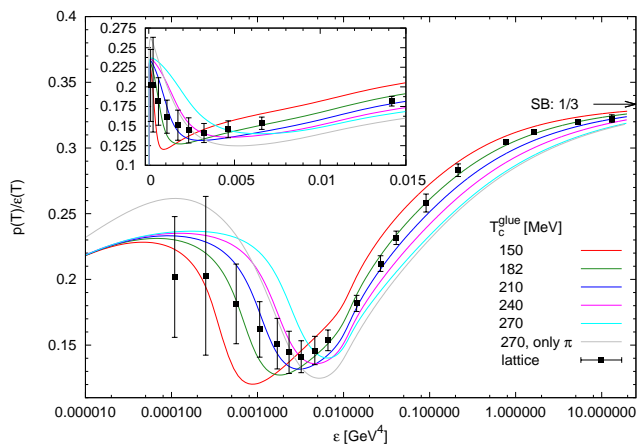


FIG. 5. The ratio p/ϵ as a function of the energy density obtained using the improved Polyakov loop potential at different values of T_c^{glue} . Unless indicated otherwise, the contribution of π , K , and f_0^L is taken into account in the grand potential. Note the logarithmic scale of the abscissa in the main plot. The inset zooms into the region of small ϵ .

sound $c_s^2(t)$ in Fig. 6 ($t = T/T_c - 1$ is the reduced temperature) turn out to be too high and too low, respectively. With the improved Polyakov loop potential the trend of the corresponding continuum extrapolated lattice results are fairly well reproduced by our results. As far as the mesonic sector is concerned, the presented quantities are basically pion dominated; however, the lattice results are better reproduced if the contributions of kaons and f_0^L are taken into account. One observes in Figs. 5 and 6 that at high temperature both c_s^2 and p/ϵ approach $1/3$, which is the value obtained in the Stefan-Boltzmann limit of the QCD.

We also studied the effect of the transition tempera-

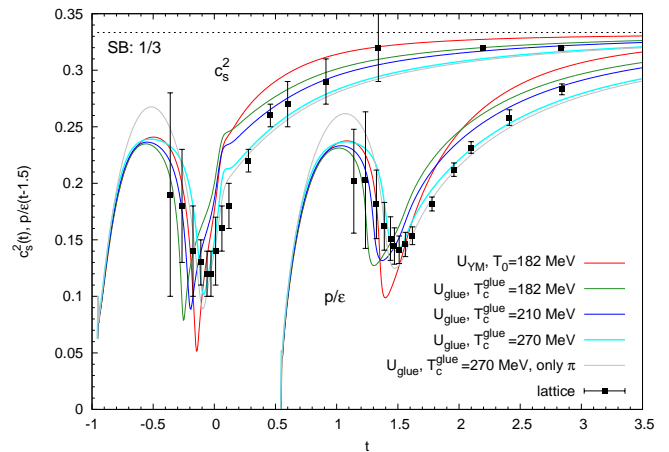


FIG. 6. The square of the speed of sound c_s^2 and the ratio p/ϵ as functions of the reduced temperature $t = T/T_c - 1$ for various parametrizations of the Polyakov loop potential. Note that p/ϵ is shifted to the right by 1.5. Unless indicated otherwise, the contribution of π , K , and f_0^L is taken into account in the grand potential.

ture T_c^{glue} appearing in the improved Polyakov loop potential. As it is visible from the figures, a single value of T_c^{glue} cannot reproduce equally well the values of all the quantities determined on the lattice. In the case of the interaction measure a large value of T_c^{glue} is favored around T_c and a smaller one at large temperatures. The minimum of $c_s^2(t)$ and $p(t)/\epsilon(t)$ is well described with $T_c^{\text{glue}} \simeq 270$ MeV, while the minimum of p/ϵ plotted as a function of ϵ is fairly well reproduced with a different value, $T_c^{\text{glue}} \simeq 210$ MeV.

C. $\mu_B - T$ phase diagram and the critical endpoint

We turn now to the study of the chiral phase transition at finite baryon chemical potential μ_B . As μ_B is increased from zero, the chiral transition as a function of the temperature becomes more and more rapid, although its crossover nature is preserved for quite large values of μ_B . The pseudocritical temperature decreases with increasing μ_B and one can determine at $\mu_B = 0$ the curvature κ of the chiral crossover transition curve in the $T - \mu_B$ plane through the following standard fit

$$\frac{T_c(\mu_B)}{T_c(\mu_B = 0)} = 1 - \kappa \left(\frac{\mu_B}{T_c(\mu_B)} \right)^2. \quad (46)$$

We obtain $\kappa = 0.0193$, which is very close to the continuum extrapolated lattice result $\kappa = 0.020(4)$ reported in [54] for the case $\mu_u = \mu_d = \mu_s$.¹⁰ We mention that when

¹⁰ We thank M. D'Elia for indicating the appropriate reference to compare our result with.

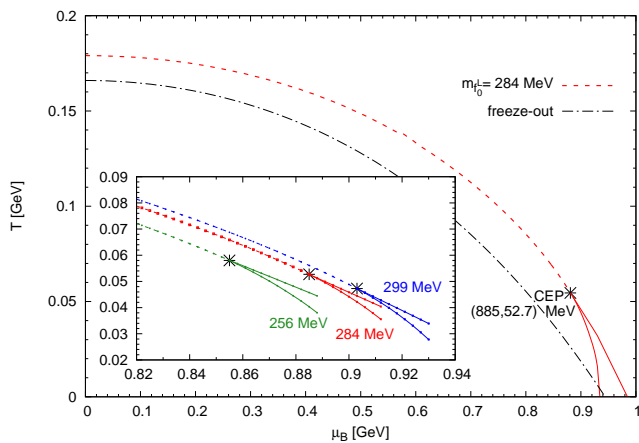


FIG. 7. The phase diagram obtained by using the improved Polyakov loop potential U_{glue} with $T_c^{\text{glue}} = 210$ MeV. The inset shows the dependence of the CEP's location on m_f^L . The dashed curve denotes a crossover-type transition, the solid curves represent the two spinodals limiting the metastable region associated with a first order phase transition, while the dash-dotted curve is the chemical freeze-out curve of Ref. [58] (see text for details).

$\mu_u = \mu_d$ and $\mu_s = 0$, the lattice results are significantly lower: $\kappa = 0.0135(20)$ in [55] and $\kappa = 0.0149(21)$ in [56].

In the case of our best set of parameters determined in Sec. IV, the crossover transition eventually turns with increasing μ_B into a first order one, by passing through the CEP of the phase boundary, where the transition is second order. This is presented in Fig. 7, where we show the phase diagram obtained with the improved Polyakov loop potential (17) by using $T_c^{\text{glue}} = 210$ MeV. The crossover transition curve can be parametrized as $T_c(\mu_B) = T_c(\mu_B = 0) - 0.101\mu_B^2 - 0.073\mu_B^4$ with $T_c(\mu_B = 0) = 0.179$ GeV. Since it was argued in [57] that the chemical freeze-out temperature is close to the critical temperature, it is interesting to compare the above transition curve with the chemical freeze-out curve deduced from particle multiplicities in heavy ion collisions, to which the parametrization $T = 0.166 - 0.139\mu_B^2 - 0.053\mu_B^4$ was given in [58], with T and μ_B measured in GeV. One can see in Fig. 7 that our $T_c(\mu_B)$ phase transition curve lies farther from the origin of the $T - \mu_B$ plane than the freeze-out curve.

With the best set of parameters given in Table IV, the location of the CEP in our model is given by $(\mu_B^{\text{CEP}}, T_c^{\text{CEP}}) = (885, 52.7)$ MeV when the improved Polyakov loop potential is used with $T_c^{\text{glue}} = 210$ MeV. The phase diagram is similar to that obtained in [59], with comparable values of the CEP's coordinates, and we refer to that paper concerning the influence of the improvement in the Polyakov loop potential on the location of the CEP in the PLσM. The large value of μ_B^{CEP} we obtained is typical of a linear sigma model without (axial)vector mesons in the case when the vacuum fluctuation of the fermions is included. See, e.g., [7] where the

value $\mu_B^{\text{CEP}} = 849$ MeV was reported, with a somewhat larger value of temperature, $T_c^{\text{CEP}} = 81$ MeV, than is in our case. Without the inclusion of the fermionic vacuum fluctuations, as is the case of Refs. [6, 60], the value of μ_B^{CEP} is smaller and T_c^{CEP} higher, compared to the case when they are properly taken into account. In Fig. 7 of [7] one can see that the inclusion of the fermionic vacuum fluctuations shifts the CEP found for $m_\sigma = 400$ MeV at $(\mu_B^{\text{CEP}}, T_c^{\text{CEP}}) = (240, 177.5)$ MeV to the location quoted above, that is $\mu_B^{\text{CEP}}/T_c^{\text{CEP}}$ increases from 1.35 to 10.5.

The continuum extrapolated lattice results of [56], obtained using analytical continuation from imaginary chemical potential, show no evidence of CEP up to $\mu_B \approx 350$ MeV. Although there exist lattice estimates on the location of the CEP, these are obtained at fixed lattice spacing and temporal extent $N_t = 4$ and at different numbers of flavors ($N_f = 2$ and $N_f = 2 + 1$), value of the pion mass, and lattice volume (see Table I of [61]). Opposed to these is the lattice result [62] obtained at $N_t = 4$, in which the shrinking of the first order chiral transition region of the $m_{u,d} - m_s$ plane was observed as μ_B is increased from zero. The result of Ref. [62] would suggest the absence of CEP, unless the $\mu_B^{\text{crit}}(m_{u,d}, m_s)$ surface of the second order phase transition points behaves nonmonotonously with increasing μ_B , similar to the situation observed, e.g., in [63] in the Nambu-Jona-Lasinio model, using a μ_B -dependent 't Hooft coupling, or in [64], in the linear sigma model.

Instead of comparing the location of the CEP found in our model to lattice results obtained at fixed lattice spacing, we compare it with values coming from the solutions of truncated Dyson-Schwinger equations in Landau gauge QCD obtained with $N_f = 2$ [65–67] and with $N_f = 2 + 1$ [68, 69], and also with an estimate obtained by analyzing experimental data in heavy-ion collisions [71]. Simple parametrizations of the gluon propagator gives $\mu_B^{\text{CEP}}/T_c^{\text{CEP}} \simeq 3.3$ in [65], which does not seem to depend on the dressing of the quark-gluon vertex, and $\mu_B^{\text{CEP}}/T_c^{\text{CEP}} \simeq 3.4$ in [66]. On the other hand, when a temperature dependent parametrization of the gluon propagator is used in [67], based on which the T dependence of the quark-antiquark condensate is reproduced at $\mu_B = 0$, $\mu_B^{\text{CEP}}/T_c^{\text{CEP}} \simeq 6.8$ is obtained, which is a factor of 2.5 smaller than our value and a factor of 2 larger than the values in [65, 66]. Compared to these values, $\mu_B^{\text{CEP}}/T_c^{\text{CEP}} \simeq 4.4$ was found in [68] (our value of μ_B^{CEP} is 1.75 times larger and our value of T_c^{CEP} is 2 times smaller than there), which increases slightly to 4.7 [69] with the inclusion of terms in the quark-gluon interaction which are parametrized with baryonic degrees of freedom. What is common in the approach based on the Dyson-Schwinger equations and also in the method of [70]¹¹ using finite energy sum rules is that they rely on the self-consistent propagator equation for the quarks.

¹¹ We thank the referee for bringing this reference and also Ref. [67] to our attention. Note that in [70] no CEP was found for $\mu_B \leq$

It remains to be seen how self-energy correction in the fermion propagator will affect in our model the value of $\mu_B^{\text{CEP}}/T_c^{\text{CEP}}$.

Recently the nonmonotonic pattern of some experimental observable obtained at various centralities as a function of the collision energy was attributed in [71] to finite-size scaling effects occurring near a second order phase transition. The determined critical exponents governing the growth of the correlation length and susceptibility suggests the existence of a CEP that belongs to the universality class of a three-dimensional Ising model and has a small value of baryon chemical potential, $\mu_B^{\text{CEP}} \approx 95$ MeV, and a high value of critical temperature $T_c^{\text{CEP}} \approx 165$ MeV.

In the inset of Fig. 7 we show the variation of the CEP's location with the value of the $\sigma \equiv f_0^L$ mass. Increasing values of the mass push the position of the CEP to higher values of μ_B and lower values of the temperature, as was observed previously in the literature in cases when only the scalar and pseudoscalar mesons were incorporated in the model, both without or with the inclusion of the fermionic vacuum fluctuations; see [6] and [7], respectively. In our case, it turned out that there is no CEP when the value of $m_{f_0^L}$ is pushed beyond ≈ 340 MeV. For changing the f_0^L mass artificially we increased the weight of the f_0^L mass in the χ^2 fit from 1 to 20, which forced the fit to reach the desired mass value. We set multiple values in the 220 – 500 MeV mass range. Even if we increased the mass weight to 20 the resulting f_0^L mass could differ from its prescribed value significantly. Finally, we ended up with two additional distinct mass values (256 MeV and 299 MeV) for which the CEP exist, as shown in Fig. 7.

D. Thermodynamical quantities at $\mu_B \neq 0$

In the previous subsection we have located the CEP in the $T - \mu_B$ phase diagram by monitoring the temperature evolution of the nonstrange condensate at increasing values of the baryon chemical potential μ_B . Now we present in Fig. 8 the temperature evolution of various thermodynamical observables at increasing values of $\mu_q = \mu_B/3$, as the CEP is approached from the region of the phase diagram where the chiral transition is an analytic crossover. Some of these observables have a peculiar behavior in the vicinity of a second order phase transition, some others increase and diverge at the CEP and therefore in principle they can be used in an experimental setting to signal its presence.

We see in Fig. 8 that the presence of the CEP is signaled by the nonmonotonic temperature dependence of the scaled pressure p/T^4 . If the pressure is scaled with

the pressure of the QCD in the SB limit, namely, by

$$p_{SB}(T, \mu_q) = (N_c^2 - 1) \frac{\pi^2}{45} T^4 + N_c N_f \left[\frac{7\pi^2}{180} T^4 + \frac{T^2 \mu_q^2}{6} + \frac{\mu_q^4}{12\pi^2} \right], \quad (47)$$

where N_c and N_f are, respectively, the number of colors and flavors, then the presence of the CEP is hardly visible. The effect of the CEP appears magnified in the scaled quark number susceptibility χ_q/T^2 and the scaled quark number density ρ_q/T^3 . Note that by increasing μ_q from 270 MeV to 289 MeV, which is very close to the coordinate of the CEP, the value of the scaled quark number susceptibility is increased by a factor of 4 (for the sake of the presentation we divided by this factor the value of χ_q/T^2 obtained at $\mu_q = 289$ MeV).

In the bottom row of Fig. 8 we show at several fixed values of μ_q the temperature variation of p/ϵ and $(dp/d\epsilon)_{\mu_q} = s/(T(\partial s/\partial T) + \mu_q(\partial \rho_q/\partial T))$. This quantity, derived at constant μ_q , connects at $\mu_q = 0$ with the square of the speed of sound c_s^2 . One sees that both p/ϵ and $(dp/d\epsilon)_{\mu_q}$ decrease with increasing values of μ_q , and that the minimum of the latter quantity approaches zero at CEP and shows a very steep rise, as the temperature increases above the critical value.

VI. CONCLUSIONS

We have studied at finite temperature and baryonic densities the thermodynamical properties of the Polyakov loop extended quark meson model containing also vector and axial vector mesons. These latter ingredients manifest themselves in a nontrivial way in the vacuum parametrization of the model through their tree-level masses and decay widths. The χ^2 -minimization procedure applied earlier in [1] was modified by including the effect of the fermion vacuum fluctuations in the scalar and pseudoscalar meson curvature masses and also by considering as an input the well-established value of the chiral transition temperature of the QCD at vanishing density.

With our parametrization procedure we have investigated which scalar particles with mass below 2 GeV can be assigned to the scalar states of the model, under the assumption that these are $q\bar{q}$ states. It turned out that the smallest value of χ^2 is reached when the states of the model correspond to $a_0(980)$, $K_0^*(800)$, $f_0(500)$, and $f_0(980)$ particles. For this particular particle assignment we have studied the thermodynamics of the model, by using an improved Polyakov loop potential, recently proposed in the literature, and found that a CEP of the crossover transition line exists in the $T - \mu_B$ phase diagram at rather large values of μ_B . We have computed various thermodynamical observables and compared them with continuum extrapolated lattice results. Based on the fairly good agreement with the lattice data observed

0.3 GeV, that is, in the range of μ_B where the approximation used is valid.

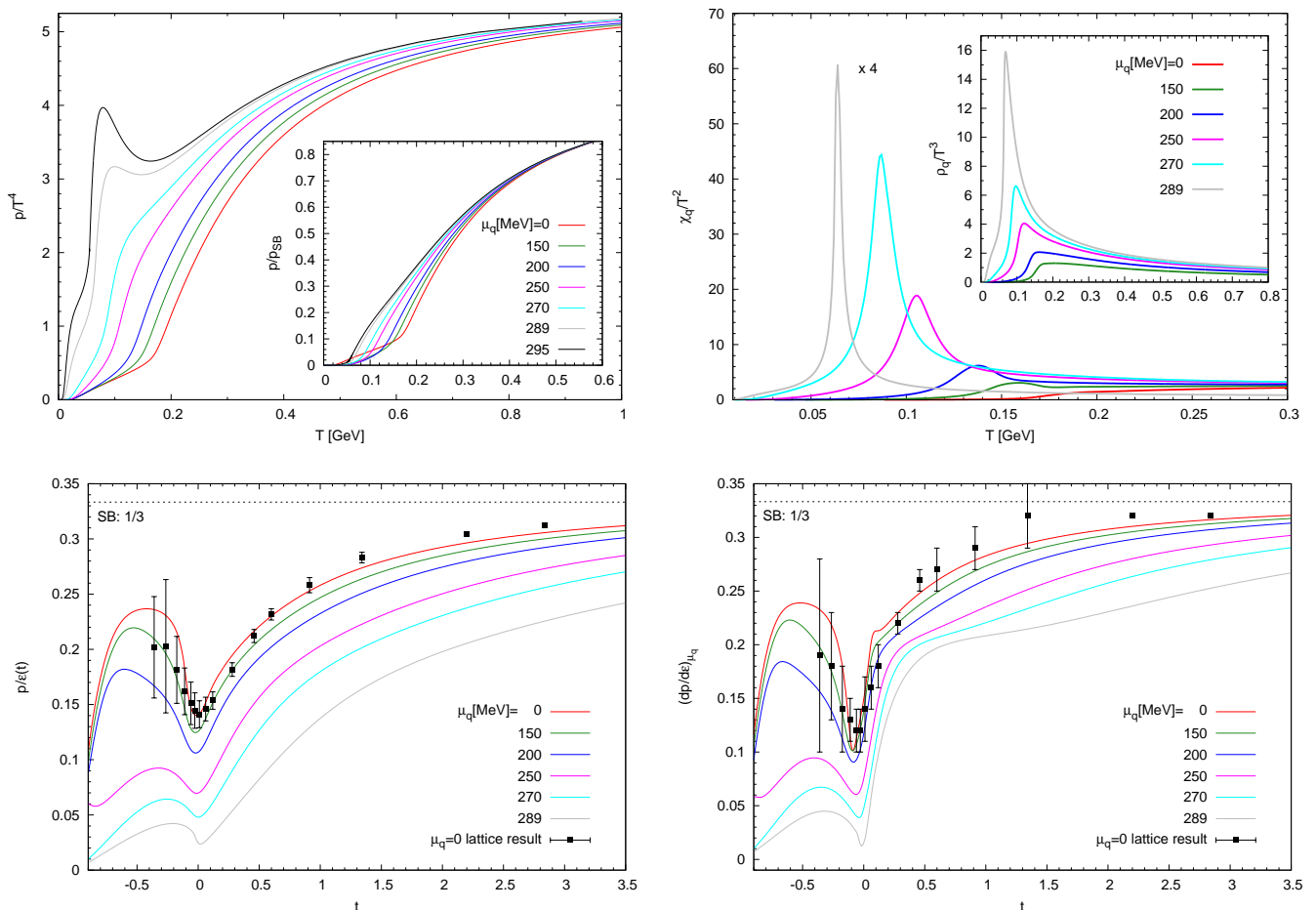


FIG. 8. The temperature dependence of thermodynamical observables at various values of quark chemical potential μ_q obtained by using the improved Polyakov loop potential U_{glue} with $T_c^{\text{glue}} = 270$ MeV and by taking into account the contribution of π , K , and f_0^L in the pressure. In the top row we show the scaled pressure p/T^4 (left main plot) and p/p_{SB} (inset), scaled quark number susceptibility χ_q/T^2 (right main plot), and the scaled quark number density ρ_q/T^3 (inset). In the bottom row we present the ratio p/ϵ and the quantity $(dp/d\epsilon)_{\mu_q}$, defined in the main text, as functions of the reduced temperature $t = T/T_c - 1$.

at vanishing density, it would be interesting to use in astrophysical applications the finite density equation of state of our model.

The inclusion of the pseudocritical temperature in the parametrization procedure proved crucial, as it drastically reduced the number of acceptable solutions of the χ^2 -minimization procedure. It turned out that in order for the model to provide a meaningful thermodynamics, $f_0(500)$ has to be part of the scalar multiplet, in contrast with the parametrization based exclusively on mesonic vacuum quantities [1], where, in the absence of fermionic vacuum fluctuations, $f_0(1370)$ and $f_0(1710)$ were found to belong to the scalar nonet states. This contradiction is most probably a consequence of the fact that in both cases the parametrization of the model was done as if the scalar states were all $\bar{q}q$ excitations, which is more likely not the case in nature. Therefore, it would be interesting to consider in the future the mixing of the $\bar{q}q$ states with tetraquark states and redo the parametrization of the model and the thermodynamical investigation pre-

sented here. We mention that additional details on the properties of some scalar particles recently given in [72–75] can also be considered in a future work. Moreover, beside the tetraquarks, the glueball admixture presumably existing in some components of the isoscalar sector [76, 77] also has to be taken into account because, as a result of the mixing of the isoscalar states, this admixture can influence the results presented here.

ACKNOWLEDGMENTS

The authors were supported by the Hungarian Research Fund (OTKA) under Contract No. K109462 and by the HIC for FAIR Guest Funds of the Goethe University Frankfurt. Zs. Sz. would like to thank Anja Habersetter for many valuable discussions which gave him insight into various technical and physical aspects of the EL σ M. P. K. and Zs. Sz. would like to thank Péter Ván and Antal Jakóvác, respectively, for helpful discussions

concerning thermodynamical observables.

Appendix A: Scalar decay widths

In this appendix the expressions of the scalar decays are listed, which are used in the parametrization and have been changed compared to [1] due to the change of the anomaly term ($\propto c_1$) in Eq. (1). The affected decays are Γ_{a_0} (this is the sum of the following three decay widths: $\Gamma_{a_0 \rightarrow \eta\pi}$, $\Gamma_{a_0 \rightarrow \eta'\pi}$, and $\Gamma_{a_0 \rightarrow KK}$), $\Gamma_{K_0^* \rightarrow K\pi}$, $\Gamma_{f_0^{L/H} \rightarrow \pi\pi}$, and $\Gamma_{f_0^{L/H} \rightarrow KK}$.

The tree-level $a_0 \rightarrow \eta\pi$ as well as $a_0 \rightarrow \eta'\pi$ decay widths read

$$\Gamma_{a_0 \rightarrow \eta\pi} = \frac{1}{8m_{a_0}\pi} \left[\frac{(m_{a_0}^2 - m_\eta^2 - m_\pi^2)^2 - 4m_\eta^2 m_\pi^2}{4m_{a_0}^4} \right]^{1/2} \times |\mathcal{M}_{a_0 \rightarrow \eta\pi}|^2, \quad (\text{A1})$$

$$\Gamma_{a_0 \rightarrow \eta'\pi} = \frac{1}{8m_{a_0}\pi} \left[\frac{(m_{a_0}^2 - m_{\eta'}^2 - m_\pi^2)^2 - 4m_{\eta'}^2 m_\pi^2}{4m_{a_0}^4} \right]^{1/2} \times |\mathcal{M}_{a_0 \rightarrow \eta'\pi}|^2, \quad (\text{A2})$$

with the following transition matrix elements,

$$\mathcal{M}_{a_0 \rightarrow \eta\pi} = \cos \theta_\pi \mathcal{M}_{a_0 \rightarrow \eta_N \pi}(m_\eta) + \sin \theta_\pi \mathcal{M}_{a_0 \rightarrow \eta_S \pi}(m_\eta), \quad (\text{A3})$$

$$\mathcal{M}_{a_0 \rightarrow \eta'\pi} = \cos \theta_\pi \mathcal{M}_{a_0 \rightarrow \eta_S \pi}(m_{\eta'}) - \sin \theta_\pi \mathcal{M}_{a_0 \rightarrow \eta_N \pi}(m_{\eta'}), \quad (\text{A4})$$

where

$$\mathcal{M}_{a_0 \rightarrow \eta_N \pi}(m) = A_{a_0 \eta_N \pi} - B_{a_0 \eta_N \pi} \frac{m_{a_0}^2 - m^2 - m_\pi^2}{2} + C_{a_0 \eta_N \pi} m_{a_0}^2, \quad (\text{A5})$$

$$\mathcal{M}_{a_0 \rightarrow \eta_S \pi}(m) = A_{a_0 \eta_S \pi}, \quad (\text{A6})$$

and

$$A_{a_0 \eta_N \pi} = -Z_\pi^2 \lambda_2 \phi_N, \quad (\text{A7})$$

$$B_{a_0 \eta_N \pi} = -2 \frac{g_1^2 \phi_N}{m_{a_1}^2} \left[1 - \frac{1}{2} \frac{Z_\pi^2 \phi_N^2}{m_{a_1}^2} (h_2 - h_3) \right], \quad (\text{A8})$$

$$C_{a_0 \eta_N \pi} = g_1 Z_\pi^2 w_{a_1}, \quad (\text{A9})$$

$$A_{a_0 \eta_S \pi} = \frac{1}{2} c_1 Z_\pi Z_{\eta_S} \phi_N^2 \phi_S. \quad (\text{A10})$$

The $a_0 \rightarrow KK$ decay width is found to be

$$\Gamma_{a_0 \rightarrow KK} = \frac{1}{8m_{a_0}\pi} \sqrt{1 - \left(\frac{2m_K}{m_{a_0}} \right)^2} \left| A_{a_0 KK} - \frac{1}{2} B_{a_0 KK} (m_{a_0}^2 - 2m_K^2) + C_{a_0 KK} m_{a_0}^2 \right|^2, \quad (\text{A11})$$

where

$$A_{a_0 KK} = Z_K^2 \left(\lambda_2 \left(\phi_N - \frac{\phi_S}{\sqrt{2}} \right) + \frac{1}{4} c_1 \right), \quad (\text{A12})$$

$$B_{a_0 KK} = Z_K^2 w_{K_1} \left\{ g_1 - \frac{1}{2} w_{K_1} ((g_1^2 + h_2) \phi_N + \sqrt{2} (g_1^2 - h_3) \phi_S) \right\}, \quad (\text{A13})$$

$$C_{a_0 KK} = -\frac{g_1}{2} Z_K^2 w_{K_1}. \quad (\text{A14})$$

It is worth noting that in the expressions above only the forms of $A_{a_0 \eta_N \pi}$ and $A_{a_0 KK}$ have changed.

Now turning to the scalar kaon, the decay width reads

$$\Gamma_{K_0^* \rightarrow K\pi} = \frac{3}{8\pi m_{K_0^*}} \left[\frac{(m_{K_0^*}^2 - m_\pi^2 - m_K^2)^2 - 4m_\pi^2 m_K^2}{4m_{K_0^*}^4} \right]^{1/2} \times \left[A_{K_0^* K\pi} + \frac{1}{2} (C_{K_0^* K\pi} + D_{K_0^* K\pi} - B_{K_0^* K\pi}) \times (m_{K_0^*}^2 - m_K^2 - m_\pi^2) + C_{K_0^* K\pi} m_K^2 + D_{K_0^* K\pi} m_\pi^2 \right], \quad (\text{A15})$$

with

$$A_{K_0^* K\pi} = Z_\pi Z_K Z_{K_0^*} \left(\lambda_2 \frac{\phi_S}{\sqrt{2}} + \frac{c_1}{2} \right), \quad (\text{A16})$$

$$B_{K_0^* K\pi} = \frac{Z_\pi Z_K Z_{K_0^*}}{4} w_{a_1} w_{K_1} \left[2g_1 \frac{w_{a_1} + w_{K_1}}{w_{a_1} w_{K_1}} + (2h_3 - h_2 - 3g_1^2) \phi_N - \sqrt{2} (g_1^2 + h_2) \phi_S \right], \quad (\text{A17})$$

$$C_{K_0^* K\pi} = \frac{Z_\pi Z_K Z_{K_0^*}}{2} [-g_1 (i w_{K^*} + w_{K_1}) + \sqrt{2} i w_{K_0^*} w_{K_1} (g_1^2 - h_3) \phi_S], \quad (\text{A18})$$

$$D_{K_0^* K\pi} = \frac{Z_\pi Z_K Z_{K_0^*}}{4} [2g_1 (i w_{K_0^*} - w_{a_1}) + i w_{K_0^*} w_{a_1} \times ((2h_3 - h_2 - 3g_1^2) \phi_N + \sqrt{2} (g_1^2 + h_2) \phi_S)], \quad (\text{A19})$$

where only $A_{K_0^* K\pi}$ has changed.

The decay widths of the $f_0^{L/H}$ in the $\pi\pi$ channel are

$$\Gamma_{f_0^L \rightarrow \pi\pi} = \frac{3}{32\pi m_{f_0^L}} \sqrt{1 - \left(\frac{2m_\pi}{m_{f_0^L}} \right)^2} \left| \mathcal{M}_{f_0^L \rightarrow \pi\pi} \right|^2, \quad (\text{A20})$$

$$\Gamma_{f_0^H \rightarrow \pi\pi} = \frac{3}{32\pi m_{f_0^H}} \sqrt{1 - \left(\frac{2m_\pi}{m_{f_0^H}} \right)^2} \left| \mathcal{M}_{f_0^H \rightarrow \pi\pi} \right|^2, \quad (\text{A21})$$

where the matrix elements are

$$\mathcal{M}_{f_0^L \rightarrow \pi\pi} = -\sin \theta_\sigma \mathcal{M}_{f_0 \pi}^H(m_{f_0^L}) + \cos \theta_\sigma \mathcal{M}_{f_0 \pi}^L(m_{f_0^L}), \quad (\text{A22})$$

$$\mathcal{M}_{f_0^H \rightarrow \pi\pi} = \cos\theta_\sigma \mathcal{M}_{f_0\pi}^H(m_{f_0^H}) + \sin\theta_\sigma \mathcal{M}_{f_0\pi}^L(m_{f_0^H}), \quad (\text{A23})$$

$$\mathcal{M}_{f_0\pi}^L(m) = 2Z_\pi^2 \phi_N \left\{ \frac{g_1^2}{2} \frac{m^2}{m_{a_1}^2} \left[1 + \left(1 - \frac{2m_\pi^2}{m^2} \right) \times \frac{m_1^2 + h_1 \phi_S^2/2 + 2\delta_N}{m_{a_1}^2} \right] - \left(\lambda_1 + \frac{\lambda_2}{2} \right) \right\}, \quad (\text{A24})$$

$$\mathcal{M}_{f_0\pi}^H(m) = 2Z_\pi^2 \phi_S \left\{ -\frac{g_1^2}{4} \frac{m^2}{m_{a_1}^2} \left(1 - \frac{2m_\pi^2}{m^2} \right) \frac{h_1 \phi_N^2}{m_{a_1}^2} - \lambda_1 + \frac{c_1}{2\sqrt{2}\phi_S} \right\}. \quad (\text{A25})$$

In the KK channel the decay widths read

$$\Gamma_{f_0^H \rightarrow KK} = \frac{1}{8\pi m_{f_0^H}} \sqrt{1 - \left(\frac{2m_K}{m_{f_0^H}} \right)^2} \left| \mathcal{M}_{f_0^H \rightarrow KK} \right|^2, \quad (\text{A26})$$

$$\Gamma_{f_0^L \rightarrow KK} = \frac{1}{8\pi m_{f_0^L}} \sqrt{1 - \left(\frac{2m_K}{m_{f_0^L}} \right)^2} \left| \mathcal{M}_{f_0^L \rightarrow KK} \right|^2, \quad (\text{A27})$$

where the matrix elements, using the notations $H_N \equiv \frac{1}{4}(g_1^2 + 2h_1 + h_2)$ and $H_S \equiv \frac{1}{2}(g_1^2 + h_1 + h_2)$, are

$$\mathcal{M}_{f_0^L \rightarrow KK} = -\sin\theta_\sigma \mathcal{M}_{f_0K}^H(m_{f_0^L}) + \cos\theta_\sigma \mathcal{M}_{f_0K}^L(m_{f_0^L}), \quad (\text{A28})$$

$$\mathcal{M}_{f_0^H \rightarrow KK} = \cos\theta_\sigma \mathcal{M}_{f_0K}^H(m_{f_0^H}) + \sin\theta_\sigma \mathcal{M}_{f_0K}^L(m_{f_0^H}), \quad (\text{A29})$$

$$\mathcal{M}_{f_0K}^L(m) = -Z_K^2 \left[(2\lambda_1 + \lambda_2)\phi_N - \frac{\lambda_2}{\sqrt{2}}\phi_S + g_1 w_{K_1} (m_K^2 - m^2) + w_{K_1}^2 \left(2H_N \phi_N - \frac{h_3 - g_1^2}{\sqrt{2}} \phi_S \right) \frac{m^2 - 2m_K^2}{2} - \frac{c_1}{2} \right], \quad (\text{A30})$$

$$\mathcal{M}_{f_0K}^H(m) = -Z_K^2 \left[2(\lambda_1 + \lambda_2)\phi_S - \frac{\lambda_2}{\sqrt{2}}\phi_N + \sqrt{2}g_1 w_{K_1} (m_K^2 - m^2) + w_{K_1}^2 \left(2H_S \phi_S - \frac{h_3 - g_1^2}{\sqrt{2}} \phi_N \right) \frac{m^2 - 2m_K^2}{2} \right]. \quad (\text{A31})$$

In the $f_0^{L/H}$ decays only the $\mathcal{M}_{f_0\pi}^L(m)$ and $\mathcal{M}_{f_0K}^L(m)$ expressions have changed.

Appendix B: Experimental data and fitting results for the parametrizations

In this appendix we give all the experimental data used for the determination of the parameters. With the exception of the constituent quark masses for which we use the values from Chap. 5.5 of Ref. [40] (see Sec. IV as well), the data are taken from the PDG [2] with some

necessary modifications explained in detail in [1]. Some of the data were not used in [1] or were used differently there; these are the following: m_{a_0} , $m_{f_0(500)}$, $m_{f_0(980)}$, $\Gamma_{a_0(980)}$, $\Gamma_{f_0(500) \rightarrow \pi\pi}$, $\Gamma_{f_0(500) \rightarrow KK}$, $\Gamma_{f_0(980) \rightarrow \pi\pi}$, and $\Gamma_{f_0(980) \rightarrow KK}$, for which the values are taken from the PDG. In general we allowed for larger errors than the ones in the PDG, namely, 20% for the scalar sector, 10% for the constituent quarks, and 5% for everything else. However, if for a quantity the PDG error turned out to be larger, then we used the error value from the PDG.

The value of different quantities in the pseudoscalar and (axial)vector sector can be found in Table V. Since that table contains only a few from the many possible assignments of the scalar particles to the states of the scalar nonet, we list below all the values of scalar masses and decay widths used in the fit,

$$\begin{aligned} m_{a_0(980)} &= (980 \pm 20) \text{ MeV}, \\ \Gamma_{a_0(980)} &= (75 \pm 25) \text{ MeV}, \\ m_{a_0(1450)} &= (1474 \pm 19) \text{ MeV}, \\ \Gamma_{a_0(1450)} &= (265 \pm 13) \text{ MeV}, \\ m_{K_0^*(800)} &= (682 \pm 29) \text{ MeV}, \\ \Gamma_{K_0^*(800) \rightarrow K\pi} &= (547 \pm 24) \text{ MeV}, \\ m_{K_0^*(1430)} &= (1425 \pm 50) \text{ MeV}, \\ \Gamma_{K_0^*(1430) \rightarrow K\pi} &= (270 \pm 80) \text{ MeV}, \\ m_{f_0(500)} &= (475 \pm 75) \text{ MeV}, \\ \Gamma_{f_0(500) \rightarrow \pi\pi} &= (550 \pm 150) \text{ MeV}, \\ \Gamma_{f_0(500) \rightarrow KK} &= (0 \pm 100) \text{ MeV}, \\ m_{f_0(980)} &= (990 \pm 20) \text{ MeV}, \\ \Gamma_{f_0(980) \rightarrow \pi\pi} &= (70 \pm 30) \text{ MeV}, \\ \Gamma_{f_0(980) \rightarrow KK} &= (0 \pm 20) \text{ MeV}, \\ m_{f_0(1370)} &= (1350 \pm 150) \text{ MeV}, \\ \Gamma_{f_0(1370) \rightarrow \pi\pi} &= (250 \pm 100) \text{ MeV}, \\ \Gamma_{f_0(1370) \rightarrow KK} &\approx (150 \pm 100) \text{ MeV}, \\ m_{f_0(1500)} &= (1505 \pm 6) \text{ MeV}, \\ \Gamma_{f_0(1500) \rightarrow \pi\pi} &= (38 \pm 2.6) \text{ MeV}, \\ \Gamma_{f_0(1500) \rightarrow KK} &= (9.4 \pm 1.9) \text{ MeV}, \\ m_{f_0(1710)} &= (1722 \pm 6) \text{ MeV}, \\ \Gamma_{f_0(1710) \rightarrow \pi\pi} &= (29.3 \pm 5) \text{ MeV}, \\ \Gamma_{f_0(1710) \rightarrow KK} &= (71.4 \pm 18) \text{ MeV}. \end{aligned} \quad (\text{B1})$$

TABLE V. Experimental values of masses and decay widths and best fit results in three cases: original fit of [1] that is without fitting f_0 masses, without $\Gamma_{f_0^{L/H} \rightarrow \pi\pi/KK}$ decay widths, and with the fermions excluded from the model (left “Fit” column); best and second best solutions with the current approach explained in Sec. IV (middle and right “Fit” columns, respectively). The labels in the first row refer in order to the particle assignments of a_0 , K_0^* , and the two f_0 ’s (with low and high mass). We use the *scientific E notation* in which m_{E-n} corresponds to $m \times 10^{-n}$.

Observable	Exp. ^{2,2,N,N} [GeV]	Fit ^{2,2,N,N} [GeV]	Exp. ^{1,1,1,2} [GeV]	Fit ^{1,1,1,2} [GeV]	Exp. ^{1,1,1,3} [GeV]	Fit ^{1,1,1,3} [GeV]
f_π	$9.221_{E-2} \pm 1.6_{E-4}$	9.630_{E-2}	$9.221_{E-2} \pm 1.6_{E-4}$	9.55_{E-2}	$9.221_{E-2} \pm 1.6_{E-4}$	9.420_{E-2}
f_K	$0.1105 \pm 8.0_{E-4}$	0.1069	$0.1105 \pm 8.0_{E-4}$	0.1094	$0.1105 \pm 8.0_{E-4}$	0.1095
m_π	$0.1380 \pm 3.0_{E-3}$	0.1410	$0.1380 \pm 3.0_{E-3}$	0.1405	$0.1380 \pm 3.0_{E-3}$	0.1392
m_η	$0.54786 \pm 1.8_{E-5}$	0.5094	$0.54786 \pm 1.8_{E-5}$	0.5421	$0.54786 \pm 1.8_{E-5}$	0.5473
$m_{\eta'}$	$0.95778 \pm 6.0_{E-5}$	0.9625	$0.95778 \pm 6.0_{E-5}$	0.9643	$0.95778 \pm 6.0_{E-5}$	0.9595
m_K	$0.49564 \pm 2.0_{E-3}$	0.4856	$0.49564 \pm 2.0_{E-3}$	0.4995	$0.49564 \pm 2.0_{E-3}$	0.5076
m_ρ	$0.7753 \pm 3.4_{E-4}$	0.7831	$0.7753 \pm 3.4_{E-4}$	0.8064	$0.7753 \pm 3.4_{E-4}$	0.8021
m_ϕ	$1.019461 \pm 1.9_{E-5}$	0.9751	$1.019461 \pm 1.9_{E-5}$	0.9901	$1.019461 \pm 1.9_{E-5}$	1.0026
m_{K^*}	$0.8947 \pm 3.0_{E-4}$	0.8851	$0.8947 \pm 3.0_{E-4}$	0.9152	$0.8947 \pm 3.0_{E-4}$	0.9200
m_{a_1}	$1.2300 \pm 4.0_{E-2}$	1.186	$1.2300 \pm 4.0_{E-2}$	1.0766	$1.2300 \pm 4.0_{E-2}$	1.0773
$m_{f_1(1420)}$	$1.4264 \pm 9.0_{E-4}$	1.373	$1.4264 \pm 9.0_{E-4}$	1.4160	$1.4264 \pm 9.0_{E-4}$	1.4282
m_{a_0}	$1.4740 \pm 1.9_{E-2}$	1.363	$0.9800 \pm 2.0_{E-2}$	0.7208	$0.9800 \pm 2.0_{E-2}$	0.7656
$m_{K_0^*}$	$1.4250 \pm 5.0_{E-2}$	1.450	$0.682 \pm 2.9_{E-2}$	0.7529	$0.682 \pm 2.9_{E-2}$	0.8108
$m_{f_0^L}$	Not used	No fit	$0.475 \pm 7.5_{E-2}$	0.2837	$0.475 \pm 7.5_{E-2}$	0.2813
$m_{f_0^H}$	Not used	No fit	$0.990 \pm 2.0_{E-2}$	0.7376	1.350 ± 0.15	0.8024
$m_{u,d}$	Not used	No fit	$0.308 \pm 3.1_{E-2}$	0.3224	$0.308 \pm 3.1_{E-2}$	0.3191
m_s	Not used	No fit	$0.483 \pm 4.9_{E-2}$	0.4577	$0.483 \pm 4.9_{E-2}$	0.4513
$\Gamma_{\rho \rightarrow \pi\pi}$	$0.1491 \pm 1.1_{E-3}$	0.1609	$0.1491 \pm 1.1_{E-3}$	0.1515	$0.1491 \pm 1.1_{E-3}$	0.1505
$\Gamma_{\phi \rightarrow \bar{K}K}$	$3.545_{E-3} \pm 2.6_{E-5}$	3.340_{E-3}	$3.545_{E-3} \pm 2.6_{E-5}$	3.534_{E-3}	$3.545_{E-3} \pm 2.6_{E-5}$	3.546_{E-3}
$\Gamma_{K^* \rightarrow K\pi}$	$4.8_{E-2} \pm 1.3_{E-3}$	4.460_{E-2}	$4.8_{E-2} \pm 1.3_{E-3}$	4.777_{E-2}	$4.8_{E-2} \pm 1.3_{E-3}$	4.780_{E-2}
$\Gamma_{a_1 \rightarrow \pi\gamma}$	$6.40_{E-4} \pm 2.46_{E-4}$	6.600_{E-4}	$6.40_{E-4} \pm 2.46_{E-4}$	3.670_{E-4}	$6.40_{E-4} \pm 2.46_{E-4}$	3.220_{E-4}
$\Gamma_{a_1 \rightarrow \rho\pi}$	0.425 ± 0.175	0.5490	0.425 ± 0.175	0.1994	0.425 ± 0.175	0.2919
$\Gamma_{f_1^H \rightarrow K^*K}$	$4.45_{E-2} \pm 2.1_{E-3}$	4.46_{E-2}	$4.45_{E-2} \pm 2.1_{E-3}$	4.451_{E-2}	$4.45_{E-2} \pm 2.1_{E-3}$	4.451_{E-2}
Γ_{a_0}	$0.265 \pm 1.3_{E-2}$	0.2660	$7.5_{E-2} \pm 2.5_{E-2}$	6.834_{E-2}	$7.5_{E-2} \pm 2.5_{E-2}$	7.488_{E-2}
$\Gamma_{K_0^* \rightarrow K\pi}$	$0.27 \pm 8.0_{E-2}$	0.2850	$0.547 \pm 2.4_{E-2}$	0.6001	$0.547 \pm 2.4_{E-2}$	0.5515
$\Gamma_{f_0^L \rightarrow \pi\pi}$	Not used	No fit	0.55 ± 0.15	0.5542	0.55 ± 0.15	0.5526
$\Gamma_{f_0^L \rightarrow KK}$	Not used	No fit	0.0 ± 0.1	0.0	0.0 ± 0.10	0.0
$\Gamma_{f_0^H \rightarrow \pi\pi}$	Not used	No fit	$7.0_{E-2} \pm 3.0_{E-2}$	8.166_{E-2}	0.25 ± 0.10	0.2495
$\Gamma_{f_0^H \rightarrow KK}$	Not used	No fit	$0.0 \pm 2.0_{E-2}$	0.0	0.150 ± 0.10	0.0
$T_c(\mu_B = 0)$	Not used	No fit	$0.151 \pm 1.51_{E-2}$	0.1704	$0.151 \pm 1.51_{E-2}$	0.1678

-
- [1] D. Parganlija, P. Kovács, G. Wolf, F. Giacosa and D. H. Rischke, Phys. Rev. D **87**, 014011 (2013).
[2] J. Beringer *et al.* [Particle Data Group Collaboration], Phys. Rev. D **86**, 010001 (2012).
[3] H. X. Chen, A. Hosaka and S. L. Zhu, Phys. Rev. D **76**, 094025 (2007).
[4] H. X. Chen, A. Hosaka, H. Toki and S. L. Zhu, Phys. Rev. D **81**, 114034 (2010).
[5] T. Kojo and D. Jido, Phys. Rev. D **78**, 114005 (2008).
[6] B. J. Schaefer and M. Wagner, Phys. Rev. D **79**, 014018 (2009).
[7] S. Chatterjee and K. A. Mohan, Phys. Rev. D **85**, 074018 (2012).
[8] F. Giacosa, Phys. Rev. D **75**, 054007 (2007).
[9] V. Skokov, B. Friman, E. Nakano, K. Redlich and B.-J. Schaefer, Phys. Rev. D **82**, 034029 (2010).
[10] U. S. Gupta and V. K. Tiwari, Phys. Rev. D **85**, 014010 (2012).
[11] B. J. Schaefer and M. Wagner, Phys. Rev. D **85**, 034027 (2012).
[12] J. Eser, M. Grahl and D. H. Rischke, Phys. Rev. D **92**, 096008 (2015).
[13] S. Strüder and D. H. Rischke, Phys. Rev. D **77**, 085004 (2008).

- [14] J. M. Cornwall, R. Jackiw and E. Tomboulis, Phys. Rev. D **10**, 2428 (1974).
- [15] A. N. Tawfik and A. M. Diab, Phys. Rev. C **91**, 015204 (2015).
- [16] S. Gasiorowicz and D. A. Geffen, Rev. Mod. Phys. **41**, 531 (1969).
- [17] O. Kaymakcalan and J. Schechter, Phys. Rev. D **31** (1985) 1109.
- [18] P. Ko and S. Rudaz, Phys. Rev. D **50**, 6877 (1994).
- [19] P. Kovács and G. Wolf, Acta Phys. Polon. Supp. **6**, 853 (2013).
- [20] K. Holland and U. J. Wiese, in *At the Frontier of Particle Physics*, edited by M. Shifman (World Scientific, Singapore, 2001), Vol. 3, pp. 1909-1944.
- [21] K. Fukushima, Phys. Lett. B **591**, 277 (2004).
- [22] C. Ratti, M. A. Thaler and W. Weise, Phys. Rev. D **73**, 014019 (2006).
- [23] H. Hansen, W. M. Alberico, A. Beraudo, A. Molinari, M. Nardi and C. Ratti, Phys. Rev. D **75**, 065004 (2007).
- [24] R. D. Pisarski, Phys. Rev. D **62**, 111501 (2000).
- [25] O. Scavenius, A. Dumitru and J. T. Lenaghan, Phys. Rev. C **66**, 034903 (2002).
- [26] C. Sasaki, B. Friman and K. Redlich, Phys. Rev. D **75**, 074013 (2007).
- [27] S. Roessner, C. Ratti and W. Weise, Phys. Rev. D **75**, 034007 (2007).
- [28] L. M. Haas, R. Stiele, J. Braun, J. M. Pawłowski and J. Schaffner-Bielich, Phys. Rev. D **87**, 076004 (2013).
- [29] S. Borsányi, G. Endrődi, Z. Fodor, S. D. Katz and K. K. Szabó, JHEP **1207**, 056 (2012).
- [30] B. J. Schaefer, J. M. Pawłowski and J. Wambach, Phys. Rev. D **76**, 074023 (2007).
- [31] U. Reinosa, J. Serreau, M. Tissier and N. Wschebor, Phys. Rev. D **93**, 105002 (2016).
- [32] J. I. Kapusta and C. Gale, *Finite-Temperature Field Theory: Principles and Applications* (Cambridge University Press, Cambridge, UK, 2006).
- [33] V. K. Tiwari, Phys. Rev. D **88**, 074017 (2013).
- [34] U. S. Gupta and V. K. Tiwari, Phys. Rev. D **81**, 054019 (2010).
- [35] B. W. Mintz, R. Stiele, R. O. Ramos and J. Schaffner-Bielich, Phys. Rev. D **87**, 036004 (2013).
- [36] S. Roessner, T. Hell, C. Ratti and W. Weise, Nucl. Phys. A **814**, 118 (2008).
- [37] U. Reinosa, J. Serreau and M. Tissier, Phys. Rev. D **92**, 025021 (2015).
- [38] F. James and M. Roos, Comput. Phys. Commun. **10** (1975) 343.
- [39] F. Giacosa and G. Pagliara, Nucl. Phys. A **833**, 138 (2010).
- [40] D. Griffiths, *Introduction to elementary particles*, Weinheim, Germany: Wiley-VCH (2008).
- [41] Y. Aoki, Z. Fodor, S. D. Katz and K. K. Szabo, Phys. Lett. B **643**, 46 (2006).
- [42] S. Borsányi, Z. Fodor, C. Hoelbling, S. D. Katz, S. Krieg, C. Ratti, K. K. Szabó, JHEP **1009**, 073 (2010).
- [43] M. Cheng *et al.*, Phys. Rev. D **77**, 014511 (2008).
- [44] E. Megias, E. Ruiz Arriola and L. L. Salcedo, Phys. Rev. D **74**, 065005 (2006).
- [45] M. Oleszczuk and J. Polonyi, Annals Phys. **227**, 76 (1993).
- [46] P. Costa, M. C. Ruivo, C. A. de Sousa and Y. L. Kalinovsky, Phys. Rev. D **71**, 116002 (2005).
- [47] T. Kunihiro, Phys. Lett. B **219**, 363 (1989).
- [48] M. C. Ruivo, P. Costa and C. A. de Sousa, Phys. Rev. D **86**, 116007 (2012).
- [49] G. Markó, U. Reinosa and Z. Szép, Phys. Rev. D **87**, 105001 (2013).
- [50] J. O. Andersen, T. Brauner and W. Naylor, Phys. Rev. D **92**, 114504 (2015).
- [51] S. Borsányi, G. Endrődi, Z. Fodor, A. Jakovác, S. D. Katz, S. Krieg, C. Ratti and K. K. Szabó, JHEP **1011**, 077 (2010).
- [52] V. Skokov, B. Stokic, B. Friman and K. Redlich, Phys. Rev. C **82**, 015206 (2010).
- [53] G. Markó and Zs. Szép, Phys. Rev. D **82**, 065021 (2010).
- [54] P. Cea, L. Cosmai and A. Papa, Phys. Rev. D **93**, 014507 (2016).
- [55] C. Bonati, M. D'Elia, M. Mariti, M. Mesiti, F. Negro and F. Sanfilippo, Phys. Rev. D **92**, 054503 (2015).
- [56] R. Bellwied, S. Borsányi, Z. Fodor, J. Günther, S. D. Katz, C. Ratti and K. K. Szabó, Phys. Lett. B **751**, 559 (2015).
- [57] P. Braun-Munzinger, J. Stachel and C. Wetterich, Phys. Lett. B **596**, 61 (2004).
- [58] J. Cleymans, H. Oeschler, K. Redlich and S. Wheaton, J. Phys. G **32**, S165 (2006).
- [59] R. Stiele and J. Schaffner-Bielich, Phys. Rev. D **93**, 094014 (2016).
- [60] H. Mao, J. Jin and M. Huang, J. Phys. G **37**, 035001 (2010).
- [61] R. V. Gavai and S. Gupta, Phys. Rev. D **71**, 114014 (2005).
- [62] P. de Forcrand and O. Philipsen, JHEP **0701**, 077 (2007).
- [63] J. W. Chen, K. Fukushima, H. Kohyama, K. Ohnishi and U. Raha, Phys. Rev. D **80**, 054012 (2009).
- [64] A. Jakovác and Zs. Szép, Phys. Rev. D **82**, 125038 (2010).
- [65] S. x. Qin, L. Chang, H. Chen, Y. x. Liu and C. D. Roberts, Phys. Rev. Lett. **106**, 172301 (2011).
- [66] C. Shi, Y. L. Wang, Y. Jiang, Z. F. Cui and H. S. Zong, JHEP **1407**, 014 (2014).
- [67] E. Gutierrez, A. Ahmad, A. Ayala, A. Bashir and A. Raya, J. Phys. G **41**, 075002 (2014).
- [68] C. S. Fischer, J. Luecker and C. A. Welzbacher, Phys. Rev. D **90**, 034022 (2014).
- [69] G. Eichmann, C. S. Fischer and C. A. Welzbacher, Phys. Rev. D **93**, 034013 (2016).
- [70] A. Ayala, A. Bashir, C. A. Dominguez, E. Gutierrez, M. Loewe and A. Raya, Phys. Rev. D **84**, 056004 (2011).
- [71] R. A. Lacey, Phys. Rev. Lett. **114**, 142301 (2015).
- [72] J. R. Pelaez, arXiv:1510.00653 [hep-ph].
- [73] T. Wolkanowski, F. Giacosa and D. H. Rischke, Phys. Rev. D **93**, 014002 (2016).
- [74] T. Wolkanowski, M. Soltysiak and F. Giacosa, Nucl. Phys. B **909**, 418 (2016).
- [75] A. H. Fariborz, A. Azizi and A. Asrar, Phys. Rev. D **91**, 073013 (2015).
- [76] S. Janowski, D. Parganlija, F. Giacosa and D. H. Rischke, Phys. Rev. D **84**, 054007 (2011).
- [77] S. Janowski, F. Giacosa and D. H. Rischke, Phys. Rev. D **90**, 114005 (2014).